AD-A115 919 ROYAL AIRCRAFT ESTABLISHMENT FARNBOROUGH (ENGLAND) F/G 20/4
NUMERICAL AERODYNAMIC STUDIES OF ASYMMETRIC GUST ENTRY.(U)
JAN 82 H C GARNER
UNCLASSIFIED RAE-TR-81157 DRIC-BR-83222 NL

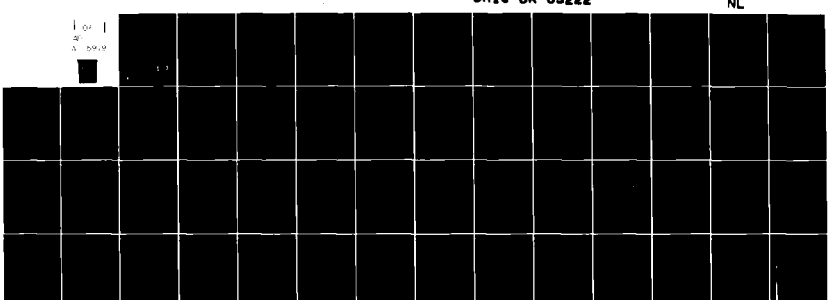

END
DATE FILMED
7 82
DTIC

TR 81157

ROYAL AIRCRAFT ESTABLISHMENT

*

Technical Report 81157

January 1982

NUMERICAL AERODYNAMIC STUDIES OF ASYMMETRIC GUST ENTRY

by

H. C. Garner

*

Procurement Executive, Ministry of Defence
Farnborough, Hants

UDC 533.6.048.5 : 533.6.013.13 : 533.693

ROYAL AIRCRAFT ESTABLISHMENT

Technical Report 81157

Received for printing 5 January 1982

NUMERICAL AERODYNAMIC STUDIES OF ASYMMETRIC GUST ENTRY

by

H. C. Garner

SUMMARY

Lifting-surface calculations for a particular wing at Mach number 0.8 are used to examine the aerodynamic consequences when one side of an aircraft enters a vertical gust before the other. The growth of lift, pitching moment, aileron hinge moment and the behaviour of the transient rolling moment are analysed. Their dependence on the inclination of the gust front and the length of a (1-cosine) gust is discussed.

Some idealized calculations of control-surface motion to suppress the wing root bending moment or to achieve undisturbed flight show only minor effects of gust inclination on control demand. But the transient rolling moment from asymmetric entry into a (1-cosine) gust within the spectrum of current airworthiness requirements is large enough to constitute a considerable handling problem. Ride control studies to eliminate heave, pitch and roll by means of two ailerons and an auxiliary tailplane or canard reveal distinct advantages of the canard as an active control.

Departmental Reference: Structures BF/B/920

LIST OF CONTENTS

1 INTRODUCTION

Airworthiness requirements for an aircraft structure include the ability to survive gust loads under prescribed conditions with an ultimate safety factor of 1.5. Aircraft are designed for discrete gust cases involving ramp or (1-cosine) gusts with velocities approaching 70 ft/s (21 m/s). Horizontal gusts are considered in order to ensure adequate stressing of the fin, while the horizontal lifting surfaces must safely bear the additional structural loads in specified vertical gusts in the absence of trimming action by the pilot.

It is sufficient to demonstrate this airworthiness quality for the aircraft in level flight at constant speed in the direction normal to the gust front. This last simplification conveniently maintains spanwise symmetry in aerodynamic loading, but in reality one wing will enter a gust before the other and the aircraft will experience rolling moment as well as pitching moment and a change in lift. The primary purpose of the present investigation is to calculate these time-dependent forces for different flight directions relative to the gust front for a step gust and also for (1-cosine) gusts.

The wing to be considered is that used in the theoretical study of active control aerodynamics in Ref 1, and the lifting-surface calculations will again be limited to the particular Mach number 0.8. The planform of aspect ratio 8 is shown in Fig 1 and includes port and starboard ailerons, which will be used as independent active controls to neutralize the rolling moment and root wing bending moment. These purely illustrative results will give some indication of the influence of asymmetry of gust entry on control demand in structural load alleviation. Pitch control will be achieved by means of an additional tailplane or canard surface, so that the three degrees of freedom in heave, pitch and roll can be considered simultaneously. The achievement of perfect ride control through a gust with three active controls is an entirely aerodynamic and somewhat academic exercise. Nevertheless, the calculated wing root bending moment will serve to illustrate how a typical structural characteristic may depend on asymmetric gust entry.

2 GROWTH OF AERODYNAMIC FORCES

The fundamentals of indicial aerodynamics in linearized compressible flow have been reviewed by Lomax[2], whose earliest references are to the classical work of Wagner[3] and Küssner[4] for two-dimensional incompressible flow. The Wagner function relates to a single abrupt change in upwash at a lifting surface, and its modern equivalent for the various aerodynamic forces due to a step change in aileron angle is used in section 3.1. We first consider the counterpart of the Küssner function for the forces on a swept wing as it enters a stationary vertical gust of constant velocity in level flight at an arbitrary inclination ψ to the normal to the gust front.

As in Ref 5, approximate estimates of lift, pitching moment and rolling moment due to asymmetric entry into a step gust can be made by means of piston theory[6]. But very few, if any, such calculations appear to have been made on the basis of lifting-surface theory. Our primary objective is to study the influence of the flight direction ψ on various Küssner functions with the aid of the subsonic lifting-surface theory of Davies[7].

2.1 Oscillatory calculations with spanwise asymmetry

Essential asymmetry in lifting-surface calculations is relatively uncommon. It has arisen in the study of acoustic propagation in Ref 8, which is focussed on the spanwise loading due to a single oscillating aileron. Antisymmetric perturbations of a symmetric mean flow are normally such that the two parts are independent, but there is a case of interaction in Ref 9 where a second-order quantity, the yawing moment due to roll rate, involves products of symmetric and antisymmetric parts of the spanwise loading.

To treat asymmetric gust entry, we first consider a sinusoidal gust with upwash velocity

$$\Re\left[we^{i\omega t}\right] = \Re\left[U \exp\left\{i\omega\left(t - \frac{x - y \tan\psi - x_0(\psi)}{U}\right)\right\}\right] , \qquad (2\text{-}1)$$

where U is the flight speed in the negative x-direction, y is to starboard, and $x_0(\psi)$ is the value of x where the gust front intersects the centre-line $y = 0$ at the moment of entry. The complex upwash angle with frequency parameter $\bar{\nu} = \omega\bar{c}/U$ is

$$\frac{w(x,y)}{U} = \cos\left[\frac{\bar{\nu}\left(x - y \tan\psi - x_0(\psi)\right)}{\bar{c}}\right] - i \sin\left[\frac{\bar{\nu}\left(x - y \tan\psi - x_0(\psi)\right)}{\bar{c}}\right] \qquad (2\text{-}2)$$

which is split into its symmetric and antisymmetric parts

$$\frac{w(x,y) + w(x,-y)}{2U} \quad \text{and} \quad \frac{w(x,y) - w(x,-y)}{2U} \qquad (2\text{-}3)$$

in preparation for the lifting-surface calculations.

Section 2.1 of Ref 1 includes some comments on calculations with the method of Davies[7]. Each force mode is written as

$$z = \Re\left[z_j(x,y)e^{i\omega t}\right] \qquad (2\text{-}4)$$

and each upwash mode as

$$\frac{w}{U} = \Re\left[\frac{w_j(x,y)}{U} e^{i\omega t}\right] . \qquad (2\text{-}5)$$

All these quantities are usually symmetric or antisymmetric in the spanwise direction. The corresponding lift per unit area

$$\Re\left[\rho U^2 \ell_j(x,y)e^{i\omega t}\right] \qquad (2\text{-}6)$$

with stream density ρ is obtained from numerical solution of an integral equation relating w_j and ℓ_j, whence the complex generalized forces are given by integrals

$$Q_{ij} = \frac{1}{\bar{c}^3}\iint z_i(x,y)\,\ell_j(x,y)\,dxdy \qquad (2\text{-}7)$$

over the planform. For our purposes it is sufficient to take integers i and j from 1 to 5. Modes 1 to 3 correspond to

$$\left.\begin{aligned} z_1 &= \bar{c} && \text{(lift)} \\ z_2 &= x - x_a && \text{(nose-down pitching moment)} \\ z_3 &= x - x_h && \text{on the aileron surfaces and zero over the rest of the planform (hinge moment)} \end{aligned}\right\}, \qquad (2\text{-}8)$$

and the corresponding upwash modes

$$\frac{w_j}{U} = \frac{\partial z_j}{\partial x} + \frac{i\omega z_j}{U} \qquad (j = 1,2,3) \qquad (2\text{-}9)$$

represent heave, pitch and symmetric aileron motion respectively. It is convenient to fix the origin of coordinates where the pitching axis intersects the centre-line (Fig 1), so that $x_a = 0$. The subscript 4 refers to antisymmetric conditions, but the force and upwash modes are unrelated. We take

$$\left.\begin{aligned} z_4 &= y && \text{(rolling moment)} \\ w_4 &= \left(y/|y|\right)w_3 && \text{(antisymmetric aileron motion)} \end{aligned}\right\}. \qquad (2\text{-}10)$$

The only other force mode to be used is the root bending moment given by

$$z_5 = |y| \quad \text{(bending moment)}, \qquad (2\text{-}11)$$

and the integer $j = 5$ denotes the sinusoidal gust, so that $w_5(x,y)$ is unconventionally asymmetric in y unless $\psi = 0$ and is given by equation (2-2). Thus the first of expressions (2-3) is used for w_5 when the force mode is symmetric ($i = 1,2,3,5$) and the second one is used for the rolling moment ($i = 4$). To obtain the separate root bending moments on the port and starboard wings, we suppose that ψ is positive and the starboard wing with y positive is the leading side relative to the gust. Let B_ℓ and B_t denote the bending moments on the leading and trailing (port) sides respectively. The rolling and total root bending moments are thus

$$\mathcal{L} = B_\ell - B_t = \rho U^2 \bar{c}^3 Q_{45} \qquad (2\text{-}12)$$

and

$$B = B_\ell + B_t = \rho U^2 \bar{c}^3 Q_{55} \qquad (2\text{-}13)$$

whence

$$\left.\begin{aligned} B_\ell &= \tfrac{1}{2}\rho U^2 \bar{c}^3 (Q_{55} + Q_{45}) \\ B_t &= \tfrac{1}{2}\rho U^2 \bar{c}^3 (Q_{55} - Q_{45}) \end{aligned}\right\}. \qquad (2\text{-}14)$$

At the outset of the lifting-surface calculations it is necessary to smooth the planform around the central and trailing-edge-crank sections (Fig 1). We follow the definitions in equations (2-7) to (2-9) of Ref 1, apart from the shift in origin to the point on the pitching axis $0.592\bar{c}$ aft of the leading apex. It is necessary also to fix the numbers of spanwise and chordwise terms in the solutions; again, following section 2.1 of Ref 1, we take respectively $m = 23$ *and* $N = 8$. Likewise, to enhance the accuracy of the solutions, we use the integers

$$q_i = (16, 8, 6, 4, 4, 6, 8, 16) \qquad (2\text{-}15)$$

of Ref 7 in evaluating w_j from the integral equation. Nevertheless, as will be seen later, the chosen value of m is not large enough to avoid minor inaccuracies.

The Mach number is fixed at $M = 0.8$, and it remains to select the frequency parameters $\bar{\nu}$ for which the complex generalized forces

$$Q_{ij}(\bar{\nu}) = Q'_{ij}(\bar{\nu}) + i\bar{\nu}Q''_{ij}(\bar{\nu}) \qquad (2\text{-}16)$$

are required. In the case of symmetric sinusoidal gusts ($j = 5$) when $\psi = 0$, the wavelength in the streamwise direction is

$$\ell_x = \frac{2\pi\bar{c}}{\bar{\nu}} , \qquad (2\text{-}17)$$

and good accuracy in superposition for the step gust is achieved by considering the range $\ell_x > \bar{c}$ or, say, $0 \leqslant \bar{\nu} \leqslant 6$. Equation (2-17) applies equally to inclined gusts, for which the wavelength in the spanwise direction

$$\ell_y = \frac{2\pi\bar{c}}{\bar{\nu}\tan\psi} = \frac{1.572s}{\bar{\nu}\tan\psi} \qquad (2\text{-}18)$$

becomes important. For example, when $\psi = 40^\circ$ and $\bar{\nu} = 6$, the number of wavelengths over the wing span is $2s/\ell_y = 6.4$ and the number of spanwise upwash points $m = 23$ is becoming inadequate. This difficulty is intensified at the larger inclinations ψ, when there is the further inconvenience that small values of $\bar{\nu}$, such as 0.01, and fairly small intervals in $\bar{\nu}$ are needed to give adequate definition to $Q_{i5}(\bar{\nu})$. For the particular case $\psi = 40^\circ$, a full set of values of the real parts Q'_{i5} is given in Table 1 for the 36 values of $\bar{\nu}$ used throughout the present calculations. Except for the hinge moment Q'_{35}, the values of Q'_{i5} for $\bar{\nu} > 3.0$ are small enough in relation to their maximum values to be almost negligible in evaluating the Küssner functions, so that inaccuracies and wide spacing in this region can be tolerated. The transient character of the rolling moment is typified by the zero value of $Q'_{45}(0)$. For each force only the first five stationary values, including that at $\bar{\nu} = 0$, are thought to matter.

2.2 Küssner functions for arbitrary gust inclination

Some detailed attention to the geometry of Fig 1 will clarify the sequence of events after the wing of leading-edge sweepback Λ_ℓ first meets the step gust at time $t = 0$. The subsequent distance of travel in mean chords is

$$\sigma = \frac{Ut}{\bar{c}} \quad . \tag{2-19}$$

When $\psi < \Lambda_\ell$ the root leading edge enters the gust at $t = 0$: when $\psi > \Lambda_\ell$ the entry of the starboard tip leading edge defines $t = 0$. For some purposes in the analysis it is convenient to use

$$\sigma_0 = \frac{U(t - t_0)}{\bar{c}} \tag{2-20}$$

where t_0 is the time at which the root leading edge enters the gust. Thus for $\psi > \Lambda_\ell$ the wing encounters the gust when

$$\sigma_0 = \sigma_e = 1.693 - 3.996 \tan \psi \quad . \tag{2-21}$$

The root trailing edge enters the gust when $\sigma_0 = 1.690$, but the wing does not become fully immersed until the port tip trailing edge enters the gust. The gust penetration along the centre-line then defines

$$\sigma_0 = \sigma_f = 2.171 + 3.996 \tan \psi \quad , \tag{2-22}$$

after which the whole wing is at uniform incidence α_g, say, and the aerodynamic loading $\rho U^2 \ell_g(x,y)$ due to the gust begins to settle to a steady state. The values of $x_0(\psi)/\bar{c}$ to be used in equation (2-2) for $w = w_s$ are identified with $(\sigma_e - 0.592)$, so that

$$\left.\begin{aligned} \frac{x_0(\psi)}{\bar{c}} &= -0.592 && (0 \leqslant \psi \leqslant \Lambda_\ell) \\ &= 1.101 - 3.996 \tan \psi && (\Lambda_\ell \leqslant \psi < 90^\circ) \end{aligned}\right\} \quad . \tag{2-23}$$

Equations (41a) and (41b) of Ref 2 give alternative expressions for the time-dependent force

$$Q_{ig} = \frac{1}{\bar{c}^3} \iint z_i(x,y)\, \ell_g(x,y)\, dxdy \tag{2-24}$$

integrated over the planform. In the present notation these alternatives are

$$Q_{ig}(\sigma) = \frac{2\alpha_g}{\pi} \int_0^\infty \frac{Q'_{i5}(\bar{\nu}) \sin \bar{\nu}\sigma}{\bar{\nu}}\, d\bar{\nu} \tag{2-25}$$

and

$$Q_{ig}(\sigma) = \alpha_g \left[Q'_{i5}(0) + \frac{2}{\pi} \int_0^\infty Q''_{i5}(\bar{\nu}) \cos \bar{\nu}\sigma \, d\bar{\nu} \right] \quad . \tag{2-26}$$

81157

Whereas equation (2-25) gives precisely $Q_{ig}(0) = 0$, equation (2-26) gives an identity in the limit as $\sigma \to 0$ which does not quite give zero after numerical integration. The present calculations are based on equation (2-25), for which a Fortran program has been

written. Because of the oscillatory behaviour of both factors in the numerator of the integrand at large $\bar{\nu}$ there is no significant error in truncating the upper limit of integration at a suitably large value. In fact, we select $\bar{\nu} = 6$ and use the 36 values in Table 1 to define $Q'_{i5}(\bar{\nu})$ by a cubic spline. The optimum choice of upper limit calls for judgement as to where the inaccuracies in the calculated $Q'_{i5}(\bar{\nu})$ have grown to the extent that it is better to replace it by zero. At the value $\sigma = 15$, say, the curve of $Q_{ig}(\sigma)$ is faired into the asymptotic expansion

$$Q_{ig}(\sigma) \approx Q'_{i5}(0) + \frac{Q'_{i5}(0)Q'_{i2}(0)}{8\pi\sigma^2} + O(\sigma^{-3}) \quad , \tag{2-27}$$

which can be reconciled with equation (38) of Ref 5 and is closely related to equation (3-30) of Ref 1. Without this facility the numerical integration, as programmed, would become inaccurate at larger values of σ because of the increasingly rapid variations in $\sin \bar{\nu}\sigma$.

The scope of the calculations of $Q_{ig}(\sigma)$ includes lift and the pitching, rolling, bending and hinge moments for ten inclinations of the gust front in the range $0 \leqslant \psi \leqslant 85^\circ$. The inaccuracies associated with high $\bar{\nu}$ begin to show themselves for small σ, but they remain very small until at $\psi = 70^\circ$ minor effects obtrude in the applications of section 3. Only limited use can be made of the results for $\psi = 80^\circ$ and 85°, where the considerations in equation (2-18) seriously question the adequacy of $m = 23$ at, say, $\bar{\nu} = 1$ where only very small errors can be tolerated. The set of results for $\psi = 40^\circ$ is given in Table 2; for this inclination trivial discrepancies appear as negative values of the bending and hinge moments on the trailing (port) side of the wing when $1.4 \leqslant \sigma \leqslant 2.0$, and the hinge moments are restricted to two decimal places.

For lift and for pitching, bending and hinge moments the quantities in Table 2 are the Küssner functions defined as

$$K_i(\sigma) = \frac{Q_{ig}(\sigma)}{Q_{ig}(\infty)} = \frac{2}{\pi}\int_0^6 \frac{Q'_{i5}(\bar{\nu})\ \sin \bar{\nu}\sigma}{Q'_{i5}\ (0)\bar{\nu}}\, d\bar{\nu} \qquad (i = 1,2,3,5) \tag{2-28}$$

from equation (2-25) with truncated integration. By means of equations (2-14) for bending moment and corresponding ones for hinge moment $K_5(\sigma)$ and $K_3(\sigma)$ are determined separately for the leading and trailing sides of the wing. As would be expected, the bending moment on the leading side grows more rapidly than the lift or pitching moment. On the trailing side the bending moment does not start to develop until after $\sigma = -\sigma_e = 1.66$ when the port wing starts to penetrate the gust. The rapid growth in hinge moment on the trailing side somewhat anticipates the arrival of the gust front at the aileron corner at $\sigma = 6.05$ and is virtually complete by $\sigma = \sigma_f - \sigma_e = 7.18$ when the aileron is fully immersed.

The rolling moment ($i = 4$), being an antisymmetric aerodynamic characteristic, is distinctive in two respects. In the first place it is transient because $Q'_{45}(0) = 0$; the quantity $Q_{4g}(\sigma)$ is therefore normalized with respect to the steady lift to give the function

$$K_4(\sigma) = \frac{Q_{4g}(\sigma)}{Q_{1g}(\infty)} = \frac{2}{\pi}\int_0^6 \frac{Q'_{45}(\bar{v})\ \sin\ \bar{v}\sigma}{Q'_{15}(0)\bar{v}}\ d\bar{v} \quad . \tag{2-29}$$

The second distinction is that the quantity $Q'_{42}(0)$ occurring in equation (2-27), being the rolling moment due to low-frequency pitching motion, is identically zero. As there is no term of order σ^{-2} in the asymptotic expansion, the steady state is approached much sooner in the rolling-moment column of Table 2.

2.3 Discussion of results

The Küssner functions, excluding hinge moments, are used in idealized active control studies at $M = 0.8$ in section 3. Various aspects of the aerodynamic loading from vertical step gusts are analysed in Figs 2 to 8, with particular attention to the dependence on entry angle ψ. Fig 2 shows the position of the gust front as the lift force reaches a quarter, a half and three quarters of its final value L_0. In the symmetric case $\psi = 0$ the wing is fully immersed soon after $L = 0.5L_0$. When the angle is increased to about 20° the lift reaches $0.75L_0$ as the gust front passes the port tip, while for the most gradual case $\psi = 80^\circ$ the steady state $L = L_0$ is approached by the time the whole wing is immersed. For each of the eight inclinations in Fig 2 the condition $L = 0.5L_0$ shortly follows the instant when the root trailing edge enters the gust.

The function in equation (2-29) may be written as

$$K_4(\sigma) = \frac{\mathcal{L}}{L_0\bar{c}} \tag{2-30}$$

where $\mathcal{L}$ is the transient rolling moment due to the gust. This quantity is conveniently plotted in Fig 3 against σ_0 from equations (2-20) and (2-21), and for each value of ψ the maximum occurs fairly close to $\sigma_0 = 1.69$ at which the root trailing edge enters the gust. This maximum grows rapidly as ψ increases from zero. The steepest gradient in $\mathcal{L}$ against σ_0 occurs soon after entry when ψ approximately equals the angle of sweepback $\Lambda_i = 23^\circ$, above which the curves become progressively more gentle and values outside the range $\sigma_e \leqslant \sigma_0 \leqslant \sigma_f$ soon become negligible. The spanwise centre of pressure as a fraction of wing semi-span

$$\bar{\eta} = \frac{\mathcal{L}}{Ls} = \frac{K_4(\sigma)\bar{c}}{K_1(\sigma)s}$$

$$= 0.2502\,\frac{K_4(\sigma)}{K_1(\sigma)} \tag{2-31}$$

is plotted against σ_0 in Fig 4. The calculations become indeterminate when σ_0 is too close to the entry value σ_e, and the curves of $\bar{\eta}$ have been smoothed to zero for $\psi < \Lambda_i$ and to unity for $\psi > \Lambda_i$. The curves for the latter range of ψ all pass fairly close to a point $(\bar{\eta},\sigma_0) = (0.38,0.8)$ as $\bar{\eta}$ is decreasing towards zero for large σ_0.

A few calculations have been made to compare the gust forces with values computed from piston theory[6], which has considerable qualitative merit. The curves of $\mathcal{L}/(L_0\bar{c})$ from piston theory in Fig 5 and from lifting-surface theory in Fig 3 have the same

general trends. Fig 6 shows for $\psi = 40^{\circ}$ that piston theory determines the spanwise centre of pressure $\bar{\eta}$ well enough. Calculations of the chordwise centre of pressure

$$\frac{\bar{x}}{\bar{c}} = \frac{Q_{2g}(\sigma)}{Q_{1g}(\sigma)} = 0.4135 \frac{K_2(\sigma)}{K_1(\sigma)} \qquad (2\text{-}32)$$

relative to the pitching axis by piston theory correctly predict a minimum in $\bar{x}/\bar{c}$ against σ_0 due to lift growth near the leading apex. But it is recognised in Figs 5 and 6 that piston theory is a poor approximation to lifting-surface theory in exaggerating the peak rolling moments by factors ranging from 1.3 to 2.2 and seriously overestimating L/L_0 and $\bar{x}/\bar{c}$. Tabulated comparisons of the lift ratio in Table 3 show maximum discrepancies that fall from 0.43 to 0.11 as ψ increases from 0 to 70°.

With the aid of equations (2-14) and $K_5(\sigma)$ and $K_4(\sigma)$ from equations (2-28) and (2-29) respectively, the Küssner functions for bending moment have been calculated separately for the two sides of the wing. These are plotted as B_ℓ/B_0 and B_t/B_0 against σ_0 in Fig 7 for five values of ψ from 0 to 55°. The main effects are the steepening of the B_ℓ curve when ψ approaches Λ_ℓ and weakening gradients in B_ℓ as ψ increases above Λ_ℓ and in B_t as ψ increases from zero. The asymptotic expression in equation (2-27), and consequently the behaviour for large σ_0 , is unaffected either by ψ or by which side of the wing is considered.

Fig 8 summarizes some of the effects of ψ and takes them to the estimated limit as ψ tends to 90°. The maximum transient rolling moment from Fig 3, the spanwise centre of pressure from Fig 4 and the half-wing bending moments from Fig 7 at the instant when $L = 0.5L_0$ are plotted against ψ . The primary consideration is the high rate at which each of these quantities varies while ψ is small. If we regard the range $0 < \psi < 20^{\circ}$ as being statistically less likely than the wider range $20^{\circ} < \psi < 90^{\circ}$, then the aerodynamic characteristics for this upper range are the more representative. They will be modified by gust length, as we shall find in section 4, but the maximum rolling moment will remain substantial.

3 NEUTRALIZATION OF GUST FORCES

In general the response to asymmetric gust entry introduces all the lateral degrees of freedom. In the present studies the ailerons are used to neutralize the rolling moment due to the gust. This idealization leads to the suppression of motion in a single antisymmetric degree of freedom in roll, and the question is how the asymmetry is likely to influence control demand or structural loading in the context of active control. As in Ref 1, perfect knowledge of the aerodynamic input from the gust is assumed without the practical consideration of sensors or control laws. We can devise two numerical studies in search of any adverse effects of the gust inclination ψ .

The first example is an idealized study of load alleviation with complete disregard of the modes of heave and pitch. The simplified problem is to determine separate movements of the two ailerons so as to eliminate simultaneously the aerodynamic root bending and rolling moments throughout the gust encounter. The influence of ψ on control demand can then be analysed.

The second numerical study simulates rise control for a rigid wing with the suppression of the forces which would cause motion in heave, pitch and roll throughout the gust encounter. To cater for the three degrees of freedom, one additional control surface is required. This third control is conceived as a tailplane or canard, which is specified simply as a lift force at a prescribed location on the centre-line $x = x_T$ or $x = x_C$. The aerodynamics of this surface are ignored in three respects, wing interference, its gust loading and the lag in growth of lift as it is deployed. With this simplification the iterative scheme of calculation embodied in equations (5-5) to (5-10) of Ref 1 will suffice to determine the time history of the two aileron angles and the control lift L_T or L_C. The objective in section 3.3 is to analyse these quantities and the residual bending moment, which plays the role of structural penalty.

3.1 Wagner functions for control surfaces

The dependence of time-dependent aerodynamic forces on the complete history of wing and control-surface motion is treated according to linearized theory in Ref 1. Several kinds of hereditary function are discussed in that paper, and in the present application we shall identify the 'hereditary velocity factor' of Ref 1 as a generalization of the Wagner function of Ref 3. Equation (2-22) of Ref 1 is therefore rewritten as

$$W_{ij}(\sigma) = 1 + \frac{2}{\pi}\int_0^\infty \frac{Q''_{ij}(\bar{\nu}) - Q''_{ij}(\infty)}{Q'_{ij}(0)} \cos \bar{\nu}\sigma \, d\bar{\nu} \quad . \tag{3-1}$$

There is an alternative expression similar to that for the Küssner function in equation (2-28), but equation (3-1) is preferable for the purposes of calculation. Section 3.3 and Appendix B of Ref 1 describe how this is evaluated by subdividing the infinite range of integration into three parts.

With application to active controls the upward displacement in the mode j is given an arbitrary smooth time dependence

$$z = q_j(\tau) z_j(x,y) \qquad (j = 1,2,3) \tag{3-2}$$

where $\tau = Ut/\bar{c}$ and z_j corresponds to equations (2-8). We shall be concerned with the symmetric aileron motion $j = 3$ and antisymmetric aileron motion $j = 4$ corresponding to w_4 in the second of equations (2-10). To avoid inconsistency in notation, the equivalent of equation (3-2) for $j = 4$ is written as

$$z = q_4(\tau)\left(\frac{y}{|y|}\right) z_3(x,y) \quad . \tag{3-3}$$

Then, following equation (2-21) of Ref 1, we shall use $W_{ij}(\sigma)$ of equation (3-1) to obtain contributions to the aerodynamic force in mode i

$$Q_i(\tau) = Q''_{ij}(\infty)\frac{dq_j(\tau)}{d\tau} + Q'_{ij}(0)\int_0^\tau \frac{dq_j(\tau_0)}{d\tau_0} W_{ij}(\tau - \tau_0)\, d\tau_0 \quad . \tag{3-4}$$

The Wagner functions for lift and the pitching, hinge, rolling and bending moments (i = 1 to 5 respectively) have been calculated for aileron motion of the configuration in Fig 1 at $M = 0.8$ and are reproduced in Table 4. As regards lift, the trailing-edge control has a more sluggish aerodynamic response than the other types, leading-edge control and all-moving tip, considered in Ref 1. The initial value $W_{13}(0) = 0.343$ is well below the value 0.5 associated with the original Wagner function for heaving velocity in two-dimensional incompressible flow. But the asymptotic expansion for large σ in three dimensions

$$W_{ij}(\sigma) \approx 1 + \frac{Q'_{1j}(0)Q'_{i2}(0)}{8\pi Q'_{ij}(0)\sigma^2} + O(\sigma^{-3}) \qquad (3\text{-}5)$$

gives a more rapid approach to the steady state than in two dimensions when there is a term of order σ^{-1}. Thus the value $W_{13}(\sigma) = 0.978$ when $\sigma = 10$ compares with the value 0.937 of the original Wagner function. The pitching moment for the particular axis responds much more rapidly than lift and gives $W_{23}(10) = 0.992$. The bending moment has intermediate characteristics so that for all σ

$$W_{13}(\sigma) < W_{53}(\sigma) < W_{23}(\sigma) \quad . \qquad (3\text{-}6)$$

The respective Wagner functions $W_{44}(\sigma)$ and $W_{33}(\sigma)$ for the rolling moment due to antisymmetric ailerons and for the symmetric hinge moment, approach the steady state much more rapidly for different reasons. Like the Küssner function $K_4(\sigma)$, $W_{44}(\sigma)$ has no term of order σ^{-2} in the asymptotic expansion (3-5) because $Q'_{14}(0) = 0$; it therefore behaves like $1 + O(\sigma^{-3})$ in Table 4. The clue to the behaviour of the symmetric hinge moment is found in the values of $-Q''_{33}(\bar{\nu})$ in Table 2 of Ref 1, which are almost constant over the range $0 < \bar{\nu} < 2$. The factor $\left[Q''_{33}(\bar{\nu}) - Q''_{33}(\infty)\right]$ in the numerator of equation (3-1) is not especially small, roughly 25% of $Q'_{33}(0)$, but the constancy of that factor in association with $\cos \bar{\nu}\sigma$ reduces the magnitude of the contribution of the integral to 0.03 or less for $\sigma > 1$. With this feature and its large initial value $W_{33}(0) = 1.908$, the hinge-moment function is strikingly different from the original Wagner function and is included in Table 4 for its intrinsic interest. The other four are required subsequently.

3.2 Load alleviation and control demand

This exercise requires the Küssner functions $K_4(\sigma)$ and $K_5(\sigma)$ for the whole range of ψ and the Wagner functions $W_{44}(\sigma)$ and $W_{53}(\sigma)$. The objective is to determine the aileron motions $q_3(\tau)$ and $q_4(\tau)$ in equations (3-2) and (3-3) so as to give quantities $Q_i(\tau)$ in equation (3-4) to neutralize the rolling and bending moments due to the step gust. From the definitions in equations (2-28) and (2-29) the integral equations

$$Q_{5g}(\infty)K_5(\tau) + Q''_{53}(\infty)\frac{dq_3(\tau)}{d\tau} + Q'_{53}(0)\int_0^\tau \frac{dq_3(\tau_0)}{d\tau_0} W_{53}(\tau - \tau_0)d\tau_0 = 0 \qquad (3\text{-}7)$$

and

$$Q_{1g}(\infty)K_4(\tau) + Q''_{44}(\infty)\frac{dq_4(\tau)}{d\tau} + Q'_{44}(0)\int_0^\tau \frac{dq_4(\tau_0)}{d\tau_0} W_{44}(\tau-\tau_0)d\tau_0 = 0 \qquad (3\text{-}8)$$

have to be solved for $q_3(\tau)$ amd $q_4(\tau)$. The two equations, being symmetric and anti-symmetric respectively, are independent and can each be solved by the iterative process based on equation (5-5) of Ref 1. Equation (3-7) is written in the form of a linear differential equation for $q_3^{(n+1)}(\tau)$

$$q_3^{(n+1)}(\tau) + \frac{Q''_{53}(\infty)}{Q'_{53}(0)}\frac{dq_3^{(n+1)}(\tau)}{d\tau} = -\frac{Q_{5g}(\infty)K_5(\tau)}{Q'_{53}(0)} - \int_0^\tau \frac{dq_3^{(n)}(\tau_0)}{d\tau_0}\left\{W_{53}(\tau-\tau_0) - 1\right\}d\tau_0 \ , \qquad \ldots\ldots (3\text{-}9)$$

where $q_3^{(n)}(\tau)$ is a previous approximation to $q_3(\tau)$. With initial values $q_3^{(0)}(\tau) \equiv 0$ the process is found to converge satisfactorily to $q_3(\tau) \approx q_3^{(9)}(\tau)$ after nine iterations. Equation (3-8) is solved for $q_4(\tau)$ similarly.

The following values are used in the calculations:

$$\left.\begin{aligned} Q_{5g}(\infty) &= -\alpha_g Q'_{55}(0) = 43.17\alpha_g \quad \text{for all } \psi \\ Q'_{53}(0) &= -5.386\ , \quad Q''_{53}(\infty) = -0.178 \\ Q_{1g}(\infty) &= -\alpha_g Q'_{15}(0) = 25.37\alpha_g \quad \text{for all } \psi \\ Q'_{44}(0) &= -5.113\ , \quad Q''_{44}(\infty) = -0.178 \end{aligned}\right\} \qquad (3\text{-}10)$$

where α_g is the upwash angle in radians associated with the gust. For the steady state at large time equation (3-7) or (3-9) gives

$$q_3(\infty) = -\frac{Q_{5g}(\infty)}{Q'_{53}(0)} = 8.015\alpha_g \ , \qquad (3\text{-}11)$$

and the corresponding limit from equation (3-8) is $q_4(\infty) = 0$ because $K_4(\infty) = 0$ as in Table 2. We write

$$\left.\begin{aligned} \delta_\ell(\tau) &= -q_3(\tau) - q_4(\tau) \\ \delta_t(\tau) &= -q_3(\tau) + q_4(\tau) \end{aligned}\right\} \qquad (3\text{-}12)$$

for the downward (nose-up) deflections of the ailerons in radians on the leading and trailing sides of the wing. The limiting conditions

$$\delta_\ell(\infty) = \delta_t(\infty) = -8.015\alpha_g \qquad (3\text{-}13)$$

imply nose-down deflections of both ailerons to counteract the upward bending moment due to an up-gust represented by positive α_g .

From the calculations of $\delta_\ell(\tau)$ and $\delta_t(\tau)$ for various gust inclinations in the range $0 \leqslant \psi \leqslant 80^\circ$, a few illustrative curves of $-\delta_\ell/\alpha_g$ and $-\delta_t/\alpha_g$ against the parameter of equation (2-20)

$$\sigma_0 = \tau - \frac{Ut_0}{\bar{c}} \qquad (3\text{-}14)$$

are drawn in Fig 9. The asymptotic from equation (3-13) is approached by the time $\sigma_0 = 10$ or, if $\psi > 55^\circ$, as soon as the wing is fully immersed in the gust. The curves have positive slopes everywhere, and the main influence of ψ is to steepen the curve on the leading side when $\psi = 25^\circ$, which is close to the condition $\psi = \Lambda_\ell$ when the whole leading edge of the leading side enters the gust at once. Above this on the leading side and for all ψ on the trailing side the gradients slacken with increasing ψ , and there are no adverse effects of asymmetric entry into a step gust. The primary reasons are the increasing distance of travel from gust entry to full immersion as ψ increases, $(\sigma_f - \sigma_e)$ mean chords from equations (2-21) and (2-22), and the rapid response in rolling moment from antisymmetric aileron movement, which is characterized by the disappearance of the σ^{-2} term in the asymptotic expansion (3-5) for $W_{44}(\sigma)$.

3.3 Ride control and residual bending moment

In Ref 1 there are calculations of symmetric aileron motion to neutralize the lift due to symmetric entry into a step gust. For the present wing of Fig 1 at $M = 0.8$, it is concluded in Ref 1 that the aileron motion $\delta(\tau)$ stabilizes about three times more quickly than the growth of lift $K_1(\sigma)$. The objective now is to extend that calculation to three degrees of freedom in heave, pitch and roll and to study the consequences for wing bending moment. We use the Küssner functions $K_1(\sigma)$, $K_2(\sigma)$, $K_4(\sigma)$ and $K_5(\sigma)$ from Table 2 for $\psi = 40^\circ$ and the corresponding functions for other gust inclinations and the Wagner functions $W_{13}(\sigma)$, $W_{23}(\sigma)$, $W_{44}(\sigma)$ and $W_{53}(\sigma)$ from Table 4.

The control motions are split into symmetric and antisymmetric aileron deflections $q_3(\tau)$ and $q_4(\tau)$, as in section 3.2; for the first example we introduce a tailplane to provide auxiliary lift $L_T(\tau)$ at a supposedly fixed location $x = x_T$. These three unknowns and the residual bending moment $B(\tau)$ can be obtained from separate calculations. The antisymmetric term $q_4(\tau)$ satisfies equation (3-8) and is solved iteratively from the linear differential equation

$$q_4^{(n+1)}(\tau) + \frac{Q''_{44}(\infty)}{Q'_{44}(0)} \frac{dq_4^{(n+1)}(\tau)}{d\tau} = -\frac{Q_{1g}(\infty)K_4(\tau)}{Q'_{44}(0)} - \int_0^\tau \frac{dq_4^{(n)}(\tau_0)}{d\tau_0} \left\{W_{44}(\tau - \tau_0) - 1\right\} d\tau_0 \qquad \ldots\ldots (3\text{-}15)$$

precisely as in section 3.2. To obtain $q_3(\tau)$, the corresponding process is used for the pitching moment about the axis $x = x_T$, to which the tailplane does not contribute. The appropriate Küssner and Wagner functions $K_T(\sigma)$ and $W_{T3}(\sigma)$ are simply derived from the definitions in equations (2-28) and (3-1). Remembering that for $i = 1$ and 2

$$Q_{ig}(\infty) = - Q'_{i5}(0)\alpha_g \quad , \tag{3-16}$$

we obtain

$$K_T(\sigma) = \frac{Q'_{25}(0)K_2(\sigma) - (x_T/\bar{c})Q'_{15}(0)K_1(\sigma)}{Q'_{25}(0) - (x_T/\bar{c})Q'_{15}(0)} \tag{3-17}$$

and

$$W_{T3}(\sigma) = \frac{Q'_{23}(0)W_{23}(\sigma) - (x_T/\bar{c})Q'_{13}(0)W_{13}(\sigma)}{Q'_{23}(0) - (x_T/\bar{c})Q'_{13}(0)} \quad . \tag{3-18}$$

The iterative solution for $q_3(\tau)$ follows from the equation

$$q_3^{(n+1)}(\tau) + \frac{Q''_{T3}(\infty)}{Q'_{T3}(0)} \frac{dq_3^{(n+1)}(\tau)}{d\tau} = - \frac{Q_{Tg}(\infty)K_T(\tau)}{Q'_{T3}(0)} - \int_0^\tau \frac{dq_3^{(n)}(\tau_0)}{d\tau_0} \left\{W_{T3}(\tau - \tau_0) - 1\right\} d\tau_0 \tag{3-19}$$

where from Table 1 of this paper and Table 2 of Ref 1

$$\left.\begin{aligned} Q''_{T3}(\infty) &= Q''_{23}(\infty) - \frac{x_T}{\bar{c}} Q''_{13}(\infty) = 0.051 \frac{x_T}{\bar{c}} - 0.073 \\ - \frac{Q_{Tg}(\infty)}{\alpha_g} &= Q'_{25}(0) - \frac{x_T}{\bar{c}} Q'_{15}(0) = 25.37 \frac{x_T}{\bar{c}} - 10.49 \\ Q'_{T3}(0) &= Q'_{23}(0) - \frac{x_T}{\bar{c}} Q'_{13}(0) = 1.788 \frac{x_T}{\bar{c}} - 1.884 \end{aligned}\right\} \quad . \tag{3-20}$$

Having obtained $q_3(\tau)$ and $q_4(\tau)$ after nine iterations, we evaluate $L_T(\tau)$ and $B(\tau)$ from equations (2-28) and (3-4). For the lift, which must be equated to zero,

$$\frac{L_T(\tau)}{\rho U^2 \bar{c}^2} - \alpha_g Q'_{15}(0)K_1(\tau) + Q''_{13}(\infty) \frac{dq_3(\tau)}{d\tau} + Q'_{13}(0) \int_0^\tau \frac{dq_3(\tau_0)}{d\tau_0} W_{13}(\tau - \tau_0) d\tau_0 = 0 \tag{3-21}$$

and for the residual bending moment

$$\frac{B(\tau)}{\rho U^2 \bar{c}^3} = - \alpha_g Q'_{55}(0)K_5(\tau) + Q''_{53}(\infty) \frac{dq_3(\tau)}{d\tau} + Q'_{53}(0) \int_0^\tau \frac{dq_3(\tau_0)}{d\tau_0} W_{53}(\tau - \tau_0) d\tau_0 \quad . \tag{3-22}$$

Because the rolling moment is neutralized, the bending moment consists of equal contributions B_ℓ and B_t from the two sides of the wing. The individual aileron angles δ_ℓ and δ_t are given by equations (3-12).

A typical set of results for $\psi = 40^\circ$ and $x_T = 3\bar{c}$ is listed in Table 5 for a unit down-gust $\alpha_g = -1$. The control angles δ_ℓ and δ_t are therefore positive to neutralize the negative lift due to the gust. The tailplane lift is of the opposite sign, because the centre of lift due to the gust, $\bar{x}/\bar{c}$ in Fig 6, lies forward of that due to

the aileron motion. The bending moment is very roughly proportional to $(\delta_\ell + \delta_t)$. The normalized values of lift and bending moment are L_T/L_0 and B/B_0 where the positive quantities

$$\left.\begin{aligned} L_0 &= \rho U^2 \bar{c}^2 \alpha_g Q'_{15}(0) \\ B_0 &= \rho U^2 \bar{c}^3 \alpha_g Q'_{55}(0) \end{aligned}\right\} \qquad (3\text{-}23)$$

are the steady forces on the wing at unit incidence. The limiting values as σ tends to infinity follow from equations (3-12), (3-15) and (3-19) to (3-23) which give

$$\delta_\ell(\infty) = \delta_t(\infty) = -q_3(\infty) = \frac{Q_{Tg}(\infty)}{Q'_{T3}(0)} = -\frac{[25.37(x_T/\bar{c}) - 10.49]\alpha_g}{1.788(x_T/\bar{c}) - 1.884}\ , \qquad (3\text{-}24)$$

$$\frac{L_T(\infty)}{L_0} = 1 - \frac{Q'_{13}(0)q_3(\infty)}{\alpha_g Q'_{15}(0)} = -\frac{1.145}{1.788(x_T/\bar{c}) - 1.884}\ , \qquad (3\text{-}25)$$

and

$$\frac{B(\infty)}{B_0} = -1 + \frac{Q'_{53}(0)q_3(\infty)}{\alpha_g Q'_{55}(0)} = \frac{1.377(x_T/\bar{c}) + 0.575}{1.788(x_T/\bar{c}) - 1.884}\ . \qquad (3\text{-}26)$$

An interesting feature of Table 5 is that each of the quantities δ_ℓ, δ_t, $-L_T/L_0$ and B/B_0 reaches a maximum near $\sigma = 7$ before falling to its steady limit. This is associated with the lag in the growth of lift when a trailing-edge control is deployed rapidly. The overshoot in aileron angle arises because the high limiting value in equation (3-24) when $x_E = 3\bar{c}$ demands a control rate high enough to need a significant extra boost to cope with the consequent lag in lift.

To change the tailplane to a canard it is sufficient to replace the positive quantity x_T and the subscript T, wherever they have appeared, by a negative quantity x_C and the subscript C. The introduction of the extra symbol is to emphasize that there is an intermediate regime where singularities would inhibit the consideration of active control and, in particular, values where equations (3-17), (3-18) and (3-24) to (3-26) would fail. Corresponding calculations for $\psi = 40^\circ$ and $x_C = -3\bar{c}$ in Table 6 have features in contrast to those in Table 5 with the tailplane as third control. Because the lift forces from the canard and the ailerons now act on opposite sides of that from the gust, at $\bar{x}/\bar{c}$ in Fig 6, the pitching moment can be neutralized with smaller individual lift contributions of the same sign. In consequence the bending moment is substantially reduced and the active canard is seen to be favourable to the structure. This is apparent from the static considerations inherent in equations (3-24) to (3-26). The smaller demand for control rate removes the overshoot found in Table 5 with the tailplane, so that with the canard each of the quantities δ_ℓ, δ_t, L_C/L_0 and B/B_0 is within 1% of its final value as soon as $\sigma > 9$.

The calculations covering variations in ψ, x_T and x_C are summarized in Figs 10 to 15. Fig 10 gives the behaviour of $\delta = \delta_\ell = \delta_t$ and L_T or L_C in symmetric cases that differ from those in Tables 5 and 6 in that $\psi = 0$ instead of $\psi = 40^\circ$. The limiting values in equations (3-24) and (3-25) are unchanged, but the overshoots in the tailplane case $x_T = 3\bar{c}$ are somewhat more marked. The canard case $x_C = -3\bar{c}$ is special, because the steady state is virtually reached when $\sigma_0 = 6$. The sluggishness in growth of lift due to aileron motion requires additional control rate that is just insufficient to give any overshoot. Fig 11 gives further information on the effect of ψ on control demand in the tailplane case $x_T = 3\bar{c}$. The most rapid control rate appears at $\psi = 25^\circ$, being close to $\psi = \psi_\ell$, but the increase is not large enough to aggravate the overshoot. A small overshoot remains on both sides of the wing at $\psi = 55^\circ$. At $\psi = 70^\circ$ the inaccuracies in the basic lifting-surface calculations, mentioned below equation (2-18), are thought to be responsible for the undulations in δ_ℓ and δ_t, which are only apparent for the first few mean chords of travel after gust entry at $\sigma_0 = -9.3$.

Fig 12 and the upper diagram of Fig 13 concern the influence of the location of the third control, which has been calculated for $\psi = 0$ and 40°. Curves of $-\delta_\ell/\alpha_g$ and $-\delta_t/\alpha_g$ against σ_0 for the asymmetric case are given in Fig 12, and they virtually coalesce near $\sigma_0 = 6$ in the three cases $x_C = -2\bar{c}$ and $x_T = 2\bar{c}$ and $4\bar{c}$. With the shorter tail arm the overshoot in $-\delta_\ell/\alpha_g$ is 9%, which falls to 2% when $x_T = 4\bar{c}$. In the absence of overshoot for the canard control at $x_C = -2\bar{c}$ the maximum control angles equal the limiting one $-\delta_\ell(\infty)/\alpha_g = 11.2$ from equation (3-24), which provides the curve of $-\delta_{max}/\alpha_g$ in Fig 13 with canard lift whatever the value of ψ. With tailplane lift there is slight dependence of $-\delta_{max}/\alpha_g$ on ψ because the overshoot is less at $\psi = 40^\circ$ than at $\psi = 0$. More significant by far is the reduction by a factor of 2, say, when the tailplane is replaced by a canard.

If δ_{max} is taken as a measure of control demand, the influence of asymmetric gust entry is marginally beneficial in the tailplane case. The extent of this small alleviation for $x_T = 3\bar{c}$ is shown in the lower diagram of Fig 13, where $-\delta_{max}/\alpha_g$ falls from 19.9 to the final value 18.8 as ψ increases from 0 to 90°. If the residual root wing bending moment is regarded as a structural penalty in achieving ride control, then Fig 14 again shows the influence of asymmetric gust entry to be marginally beneficial; whether a tailplane or a canard is used, B_{max} falls a little as ψ increases from zero. The overriding consideration for all ψ is that, with canard lift as opposed to tailplane lift, the residual bending moment is reduced by a factor of about $3\frac{1}{2}$. If, however, the maximum control rate

$$\dot{\delta}_{max} = \left[\frac{\partial}{\partial\sigma_0}\left(-\frac{\delta}{\alpha_g}\right)\right]_{max} \qquad (3\text{-}27)$$

is regarded as the primary influence of the gust inclination, then the peak values near $\psi = \Lambda_\ell = 23.0^\circ$ for the aileron on the leading side of the wing appear as the single adverse effect of asymmetric gust entry to emerge from the active control studies for step gusts. Fig 15 shows the extent of this phenomenon both for ride control, achieved with active ailerons and tailplane lift, and for load alleviation as discussed in section 3.2.

4 INFLUENCE OF GUST LENGTH

Effects of gust length are considered in relation to (1-cosine) profiles, which correspond to a half cycle of a sinusoidal gust. If x_g denotes the streamwise length of the gust, then in place of equation (2-2) we have an instantaneous upwash angle

$$\left.\begin{aligned} \frac{w(x,y)}{U} &= 0 && Ut - x + y\tan\psi + x_0(\psi) < 0 \\ &= \frac{\alpha_g}{2}\left\{1 - \cos\left[\frac{\pi}{x_g}\left(Ut - x + y\tan\psi + x_0(\psi)\right)\right]\right\} && 0 \leqslant Ut - x + y\tan\psi + x_0(\psi) \leqslant x_g \\ &= \alpha_g && Ut - x + y\tan\psi + x_0(\psi) > x_g \end{aligned}\right\} . \quad (4\text{-}1)$$

As x_g tends to zero, the middle region disappears to give a step gust of incidence α_g met by the wing at non-dimensional time $\tau = 0$. The (1-cosine) gust consists of elementary gusts of incidence

$$\delta\alpha = \frac{\pi\alpha_g}{2\sigma_g}\sin\left(\frac{\pi\tau_0}{\sigma_g}\right)\delta\tau_0 \qquad \text{at times} \quad 0 \leqslant \tau_0 \leqslant \sigma_g \quad (4\text{-}2)$$

where $$\sigma_g = \frac{x_g}{\bar{c}} . \quad (4\text{-}3)$$

By superposition, therefore, any function of σ corresponding to a step gust of incidence α_g and a particular inclination ψ , say the rolling moment $\mathcal{L}(\sigma)$, can be generalized to

$$\mathcal{L}(\sigma,\sigma_g) = \int_0^{\sigma_m} \frac{\pi}{2\sigma_g}\sin\left(\frac{\pi\tau_0}{\sigma_g}\right)\mathcal{L}(\sigma - \tau_0)d\tau_0 \quad (4\text{-}4)$$

where σ_m is σ or σ_g , whichever is the smaller.

By means of equation (4-4) it is a simple calculation to extend the results of Fig 3 for $\mathcal{L}/L_0\bar{c}$ in an inclined step gust to corresponding functions for (1-cosine) gusts of different length. For the particular gust inclination $\psi = 40^\circ$ at $M = 0.8$, Fig 16 shows eight curves of $\mathcal{L}/L_0\bar{c}$ against σ for gust lengths in the range $0 \leqslant \sigma_g \leqslant 60$. The inset diagram of

$$\left.\begin{aligned} \frac{\alpha}{\alpha_g} &= \tfrac{1}{2}\left[1 - \cos\left(\frac{\pi\sigma}{\sigma_g}\right)\right] && 0 \leqslant \frac{\sigma}{\sigma_g} \leqslant 1 \\ &= 1 && \frac{\sigma}{\sigma_g} > 1 \end{aligned}\right\} \quad (4\text{-}5)$$

in Fig 16 indicates the gust incidence at the starboard tip leading edge from the instant $\sigma = 0$ when it first enters the gust. The maximum rolling moment occurs after travel of about $3.5\bar{c}$ beyond the point where $\alpha = \frac{1}{2}\alpha_g$ and $\sigma = \frac{1}{2}\sigma_g$; the maximum value decreases slowly at first as σ_g increases, but when $\sigma_g = 20$ it has fallen to 34% of its value for the step gust. Fig 17 includes the curve of $\mathcal{L}_{max}/L_0\bar{c}$ against σ_g for $\psi = 40^\circ$, which is roughly proportional to σ_g^{-1} for large gust lengths and remains significant

up to $\sigma_g = 60$. Similar calculations of lift $L(\sigma,\sigma_g)$ for $\psi = 40^o$ and $0 \leqslant \sigma_g \leqslant 35$ are listed in Table 7, where the greatest spread of values occurs at $\sigma = 10$. The values of σ at which $L/L_0 = 0.25$, 0.50 and 0.75 are obtained for $0 \leqslant \sigma_g \leqslant 60$ and are plotted as nearly straight lines in Fig 17. The corresponding spanwise centres of pressure $\bar{\eta}$ for constant L/L_0 and the maximum rolling moment have the same general behaviour against σ_g in Fig 17. Their behaviour against ψ is similar to that shown in Fig 8.

The graphs in Figs 18 to 20 illustrate the softening influence of σ_g on the results of the active control studies. The control angles and tailplane lift in Figs 18 and 19 are obtained as functions of σ and σ_g from integrals analogous to equation (4-4). Fig 18 shows the gentler gradients in the two aileron angles when the load-alleviation exercise of section 3.2 is repeated for $\psi = 40^o$ and increasing values of σ_g from 0 to 35. Fig 19 illustrates the effect of σ_g on the ride-control exercise of section 3.3 in the symmetric case $\psi = 0$ with the tailplane at $x_T = 3\bar{c}$. As would be expected, the overshoot of about 6% in $-\delta/\alpha_g$ and $-L_T/L_0$ in the case of a step gust decreases as σ_g increases and has almost disappeared when $\sigma_g = 20$. The complete asymmetric active control solution, including the bending moment, is given for $M = 0.8$, $\sigma_g = 10$ and $\psi = 40^o$ in Table 8. A slight overshoot in all quantities is found near $\sigma = 16$. The influence of σ_g can be studied by comparing Table 5 for $\sigma_g = 0$ with Table 8 for $\sigma_g = 10$. When $\sigma > 25$ the differences no longer exceed one in the last decimal place. Fig 20 gives various curves of maximum control rate from equation (3-27) against σ_g . Although these show the usual behaviour proportional to σ_g^{-1} for large σ_g , the percentage decreases in $\dot{\delta}_{max}$ in the range $0 < \sigma_g < 20$ are greater than the corresponding decrease in maximum transient rolling moment in Fig 17.

It is appropriate to consider disturbances like small step gusts in discussing the implications of asymmetric gust entry for problems of active control. But the maximum transient rolling moment needs to be evaluated with reference to a typical (1-cosine) gust in the airworthiness requirements. This aspect of asymmetric gust entry is considered as part of a broader discussion in section 5.

5 SIGNIFICANCE OF ASYMMETRIC GUST ENTRY

Asymmetry in gusts poses a variety of problems. The present studies only concern horizontal surfaces in vertical gusts, but the airworthiness requirements recognise the corresponding case of a fin in a horizontal gust. Specifications in terms of a (1-cosine) gust of velocity 66 ft/s (20 m/s) and length $25\bar{c}$ have evolved empirically. This particular (1-cosine) gust is taken to be representative of the spectrum of current airworthiness requirements. More severe velocities can occur in thunderstorms and jet streams, and it is thought that shorter gradient distances occur naturally in vortex flows induced in the atmosphere. Asymmetric spanwise loading may arise from lateral variations in gust velocity, especially in relation to natural vortex flows and aircraft wakes. The particular aspect of asymmetric gust entry is one such problem where some clarification is now possible.

The present numerical studies have developed in the context of active controls and fairly small vertical gusts. The two idealized applications are to load alleviation, where the ailerons are used independently to eliminate the rolling and root-bending

moments, and to ride control, where lift and the pitching and rolling moments are neutralized by combined motion of the ailerons and a lift-producing tailplane or canard. The influence of the direction of entry into the gust is analysed, and the maximum control angles and residual loads are little changed. In the case of ride control with a tailplane, an overshoot in control angle is demanded (Fig 10) and there is a corresponding peak in the structural penalty measured by the bending moment (Fig 14). Both these overshoot effects diminish as the direction of entry becomes more inclined (Figs 13 and 14) and as the gust length increases (Fig 19); asymmetric gust entry is marginally beneficial in this respect. The only adverse effect is in relation to maximum control rate demand (Fig 15), which rises to a peak for the swept wing when the direction of entry is normal to the leading edge. More precise numerical studies could be made by considering the time-dependent aerodynamics of lifting surfaces in tandem. But the calculated influence of asymmetric gust entry is not significant enough to warrant an extended investigation into interfering surfaces and the Küssner effect on the tailplane or canard.

If the present results are applied to the (1-cosine) gust of velocity 66 ft/s (20 m/s), it is easily verified that the calculated demands on control angle and control rate are impractically high. Even for the (1-cosine) gust of length 100 ft (30.5 m), the maximum control rate in Fig 20 with neutralized wing forces and tailplane lift would exceed 1000°/s and, whatever the gust length, the aileron angles in Fig 19 would be approaching 90°. It is more to the point that asymmetric gust entry gives rise to a substantial rolling moment, whose peak value grows rapidly as the entry angle increases from zero (Figs 3 and 8). For a step gust of inclination $\psi = 40^{\circ}$ the maximum rolling moment is already 86% of its limit at $\psi = 90^{\circ}$ with precisely half the wing immersed in the gust. A further reduction from 86% to 25% is found when the gust length is increased to $25\bar{c}$ (Figs 16 and 17). Nevertheless, the maximum transient rolling moment due to a (1-cosine) gust of this length and velocity 66 ft/s (20 m/s) is equivalent to that produced by static aileron deflections of $\pm 3.4^{\circ}$ at $M = 0.8$, or larger deflections roughly proportional to $1/M$ at lower flight speeds.

The present evidence suggests that the traditional aircraft response calculations with symmetric gust entry cater for the severest structural loads. In practice there will be spanwise asymmetries as well, either from the nature of the gust itself or on account of the direction in which it is approached. The control rate demands can then be greater, and the acquisition of bending moments will differ on the port and starboard wings. The problem of aircraft control in gusts is oversimplified if all gusts are assumed to be symmetrical.

6 CONCLUSIONS

(1) Lifting-surface calculations show that the transient rolling moment due to asymmetric gust entry builds up rapidly as a function of the inclination of flight direction to the normal to the gust front.

(2) From particular calculations at $M = 0.8$ the maximum rolling moment experienced in a vertical (1-cosine) gust of velocity 66 ft/s (20 m/s) and length $25\bar{c}$ is large enough to be equivalent to that produced by static aileron deflections of $\pm 3.4^{\circ}$.

(3) Idealized calculations of the active control of structural loading and aircraft ride show marginally beneficial effects of asymmetric gust entry, the exception being the higher control rate demand when the gust front is parallel to a sweptback leading edge.

(4) From the ride control studies in three degrees of freedom with port and starboard ailerons and an auxiliary control, the use of a canard as opposed to a tailplane leads to lower control demand and a greatly reduced penalty in residual root bending moment.

Table 1

OSCILLATORY DATA FOR SINUSOIDAL GUSTS OF VARYING WAVELENGTH AND OF INCLINATION $\psi = 40^{\circ}$ at $M = 0.8$

$\bar{\nu}$	Lift	Pitching moment	Rolling moment	Bending moment	Hinge moment
	$-Q'_{15}$	$-Q'_{25}$	$-Q'_{45}$	$-Q'_{55}$	$-Q'_{35}$
0.000	25.37	10.49	0.00	43.17	0.0082
0.010	25.32	10.47	0.02	43.09	0.0082
0.020	25.19	10.42	0.09	42.84	0.0082
0.035	24.84	10.27	0.27	42.21	0.0081
0.050	24.33	10.06	0.54	41.28	0.0079
0.075	23.17	9.57	1.21	39.18	0.0076
0.100	21.71	8.96	2.12	36.51	0.0072
0.125	20.03	8.24	3.24	33.43	0.0067
0.150	18.19	7.46	4.55	30.07	0.0061
0.180	15.88	6.47	6.31	25.83	0.0054
0.210	13.55	5.45	8.22	21.55	0.0047
0.250	10.51	4.12	10.87	15.98	0.0037
0.300	7.00	2.56	14.10	9.60	0.0025
0.350	3.93	1.20	16.93	4.13	0.0014
0.400	1.37	0.10	19.10	-0.26	0.0005
0.450	-0.66	-0.72	20.40	-3.50	-0.0003
0.500	-2.18	-1.24	20.73	-5.60	-0.0008
0.600	-3.86	-1.45	18.61	-6.67	-0.0011
0.700	-4.09	-0.82	13.67	-4.50	-0.0004
0.800	-3.42	0.22	7.54	-0.65	0.0012
0.900	-2.40	1.23	1.83	3.16	0.0031
1.000	-1.53	1.85	-2.29	5.57	0.0047
1.200	-1.20	1.50	-4.29	4.65	0.0054
1.350	-1.88	0.35	-2.12	0.91	0.0034
1.500	-2.53	-0.63	-0.13	-2.37	0.0007
1.650	-2.61	-0.92	-0.09	-3.39	-0.0007
1.800	-2.12	-0.61	-1.74	-2.44	0.0001
2.100	-1.13	-0.10	-4.11	-0.89	0.0037
2.400	-1.16	-0.74	-2.07	-3.07	0.0016
2.700	-0.77	-0.73	-1.75	-3.00	0.0000
3.000	-0.11	-0.31	-2.67	-1.41	0.0018
3.600	-0.16	-0.61	-0.77	-1.83	-0.0010
4.200	-0.10	-0.36	-0.74	-0.78	-0.0008
4.800	-0.12	-0.12	-0.92	-0.18	-0.0014
5.400	-0.32	-0.22	-0.27	-0.80	-0.0022
6.000	-0.18	-0.08	-0.66	-0.43	-0.0024

Table 2

KÜSSNER FUNCTIONS FOR WING AT M = 0.8 AND GUST INCLINATION $\psi = 40^{\circ}$

σ^{+}	Lift $K_1(\sigma)$	Pitching moment $K_2(\sigma)$	Rolling moment* $K_4(\sigma)$	Bending moment $K_5(\sigma)$		Hinge moment $K_3(\sigma)$	
				Leading side	Trailing side	Leading side	Trailing side
0.0	0.000	0.000	0.000	0.000	0.000	0.00	0.00
0.2	0.005	0.012	0.018	0.021	0.000	0.11	0.00
0.5	0.019	0.047	0.066	0.078	0.000	0.39	0.00
0.8	0.046	0.103	0.144	0.170	0.001	0.71	0.00
1.1	0.081	0.160	0.233	0.273	0.000	0.77	0.00
1.4	0.124	0.208	0.314	0.368	-0.001	0.67	0.00
1.7	0.175	0.247	0.383	0.449	-0.001	0.67	0.00
2.0	0.228	0.280	0.439	0.515	0.000	0.74	-0.01
2.5	0.307	0.325	0.494	0.592	0.012	0.72	0.01
3.0	0.386	0.368	0.518	0.653	0.044	0.78	0.02
3.5	0.447	0.404	0.523	0.699	0.084	0.79	0.03
4.0	0.516	0.455	0.496	0.739	0.156	0.83	0.00
4.5	0.582	0.513	0.446	0.771	0.246	0.84	0.09
5.0	0.643	0.574	0.388	0.798	0.343	0.86	0.18
6.0	0.760	0.727	0.211	0.842	0.593	0.89	0.74
7.0	0.844	0.850	0.071	0.875	0.792	0.91	1.01
8.0	0.888	0.899	0.027	0.901	0.869	0.92	0.92
9.0	0.916	0.926	0.011	0.922	0.908	0.94	0.94
10.0	0.937	0.945	0.003	0.938	0.934	0.95	0.96
12.0	0.963	0.967	-0.001	0.961	0.962	0.97	0.97
14.0	0.977	0.979	0.000	0.976	0.976	0.98	0.98
16.0	0.985	0.986	0.000	0.985	0.985	0.99	0.99
20.0	0.993	0.993	0.000	0.993	0.993	1.00	0.99
25.0	0.996	0.996	0.000	0.997	0.996	1.00	1.00
30.0	0.998	0.998	0.000	0.998	0.998	1.00	1.00
40.0	0.999	0.999	0.000	0.999	0.999	1.00	1.00

† With reference to the root leading edge $\sigma_0 = \sigma - 1.660$.

* Normalized with respect to $L_0\bar{c} = 25.37\rho U^2\bar{c}^3$.

Table 3

KÜSSNER FUNCTION $K_1(\sigma)$ FOR LIFT FROM PISTON AND LIFTING-SURFACE THEORIES

σ	$\psi = 0$		$\psi = 25^\circ$		$\psi = 55^\circ$		$\psi = 70^\circ$	
	Piston	L-S	Piston	L-S	Piston	L-S	Piston	L-S
0.0	0.000	0.000	0.000	0.000	0.000	0.000	0.000	0.000
0.2	0.012	0.009	0.061	0.048	0.002	0.001	0.001	-0.005
0.5	0.074	0.048	0.215	0.128	0.016	0.006	0.007	-0.004
0.8	0.189	0.126	0.362	0.211	0.035	0.016	0.015	0.007
1.1	0.357	0.229	0.482	0.282	0.056	0.028	0.023	0.018
1.4	0.579	0.342	0.578	0.340	0.079	0.041	0.032	0.020
1.7	0.850	0.454	0.661	0.397	0.105	0.058	0.041	0.017
2.0	0.980	0.546	0.733	0.455	0.133	0.077	0.051	0.019
2.5	1.000	0.640	0.827	0.542	0.184	0.113	0.068	0.040
3.0	1.000	0.707	0.898	0.626	0.241	0.155	0.089	0.053
3.5	1.000	0.756	0.955	0.705	0.303	0.203	0.107	0.063
4.0	1.000	0.795	0.996	0.767	0.373	0.258	0.128	0.084
4.5	1.000	0.826	1.000	0.806	0.445	0.314	0.150	0.100
5.0	1.000	0.852	1.000	0.837	0.511	0.366	0.174	0.118
6.0	1.000	0.891	1.000	0.881	0.629	0.466	0.225	0.163
7.0	1.000	0.918	1.000	0.911	0.728	0.562	0.281	0.216
8.0	1.000	0.938	1.000	0.933	0.806	0.653	0.343	0.272
9.0	1.000	0.953	1.000	0.949	0.873	0.734	0.413	0.335
10.0	1.000	0.964	1.000	0.960	0.929	0.809	0.488	0.400
12.0	1.000	0.977	1.000	0.976	1.000	0.913	0.621	0.516
14.0	1.000	0.985	1.000	0.984	1.000	0.951	0.730	0.627
16.0	1.000	0.990	1.000	0.989	1.000	0.971	0.817	0.727
20.0	1.000	0.995	1.000	0.995	1.000	0.988	0.949	0.896
25.0	1.000	0.997	1.000	0.997	1.000	0.995	1.000	0.979
30.0	1.000	0.998	1.000	0.998	1.000	0.997	1.000	0.993
40.0	1.000	0.999	1.000	0.999	1.000	0.999	1.000	0.998

Table 4

WAGNER FUNCTIONS FOR INSTANTANEOUS AILERON DEFLECTION AT M = 0.8

σ	Lift $W_{13}(\sigma)$	Pitching moment $W_{23}(\sigma)$	Rolling moment $W_{44}(\sigma)$	Bending moment $W_{53}(\sigma)$	Hinge moment $W_{33}(\sigma)$
0.0	0.343	0.470	0.416	0.398	1.908
0.1	0.429	0.569	0.534	0.502	1.699
0.2	0.495	0.643	0.616	0.578	1.505
0.3	0.540	0.694	0.669	0.629	1.349
0.4	0.575	0.733	0.708	0.668	1.229
0.6	0.630	0.789	0.766	0.728	1.090
0.8	0.677	0.832	0.815	0.776	1.043
1.0	0.715	0.863	0.855	0.815	1.031
1.2	0.744	0.884	0.882	0.842	1.019
1.4	0.763	0.895	0.898	0.858	1.001
1.6	0.777	0.902	0.908	0.868	0.984
1.8	0.787	0.907	0.918	0.875	0.977
2.0	0.797	0.913	0.928	0.882	0.981
2.5	0.819	0.930	0.951	0.900	0.996
3.0	0.836	0.942	0.968	0.914	0.997
3.5	0.853	0.952	0.980	0.926	0.996
4.0	0.869	0.960	0.989	0.936	0.997
5.0	0.900	0.972	0.999	0.949	0.998
6.0	0.928	0.979	1.004	0.958	0.998
7.0	0.948	0.984	1.004	0.966	0.999
8.0	0.962	0.988	1.003	0.975	0.999
9.0	0.971	0.990	1.002	0.982	0.999
10.0	0.978	0.992	1.000	0.987	0.999
12.0	0.987	0.995	1.000	0.992	1.000
14.0	0.991	0.996	1.000	0.995	1.000
16.0	0.993	0.997	1.000	0.996	1.000
18.0	0.994	0.998	1.000	0.997	1.000
20.0	0.995	0.998	1.000	0.997	1.000
Steady state	$-Q'_{13}(0)$ = 1.788	$-Q'_{23}(0)$ = 1.884	$-Q'_{44}(0)$ = 5.113	$-Q'_{53}(0)$ = 5.386	$-Q'_{33}(0)$ = 0.0182

Table 5

REQUIRED AILERON ANGLES, TAILPLANE LIFT AND RESIDUAL ROOT BENDING MOMENT TO NEUTRALIZE AN INCLINED STEP DOWN-GUST

$M = 0.8$, $\psi = 40^{\circ}$, tailplane lift at $x_T/\bar{c} = 3$

σ	Control angles†		Tailplane lift*	Bending moment*
	Leading side δ_ℓ	Trailing side δ_t		
0.0	0.00	0.00	-0.000	0.000
0.2	0.23	0.00	-0.001	0.001
0.5	1.04	0.11	-0.004	0.010
0.8	2.44	0.43	-0.013	0.035
1.1	4.15	0.99	-0.026	0.084
1.4	6.02	1.95	-0.048	0.169
1.7	8.04	3.29	-0.077	0.289
2.0	9.93	4.69	-0.107	0.421
2.5	12.15	6.58	-0.149	0.615
3.0	13.90	8.31	-0.186	0.782
3.5	15.41	9.94	-0.220	0.931
4.0	16.72	11.78	-0.251	1.064
4.5	17.75	13.54	-0.278	1.177
5.0	18.54	15.05	-0.300	1.268
6.0	19.40	18.01	-0.330	1.379
7.0	19.51	19.43	-0.341	1.408
8.0	19.36	19.39	-0.340	1.400
9.0	19.21	19.23	-0.338	1.385
10.0	19.05	19.05	-0.334	1.370
12.0	18.84	18.82	-0.329	1.350
14.0	18.81	18.80	-0.328	1.348
16.0	18.84	18.84	-0.329	1.351
20.0	18.88	18.88	-0.329	1.355
25.0	18.87	18.87	-0.329	1.354
30.0	18.87	18.87	-0.329	1.354
40.0	18.86	18.86	-0.329	1.353
∞	18.86	18.86	-0.329	1.353

† Normalized with respect to gust downwash angle.

* Normalized with respect to steady magnitude on the wing corresponding to gust.

Table 6

REQUIRED AILERON ANGLES, CANARD LIFT AND RESIDUAL ROOT BENDING MOMENT TO NEUTRALIZE AN INCLINED STEP DOWN-GUST

$M = 0.8$, $\psi = 40^{\circ}$, canard lift at $x_c/\bar{c} = -3.0$

σ	Control angles†		Canard lift*	Bending moment*
	Leading side δ_ℓ	Trailing side δ_t		
0.0	0.00	0.00	0.000	0.000
0.2	0.21	-0.02	0.000	-0.002
0.5	0.90	-0.03	0.002	-0.003
0.8	2.02	0.01	0.005	-0.001
1.1	3.28	0.12	0.010	0.010
1.4	4.46	0.39	0.018	0.033
1.7	5.58	0.84	0.030	0.072
2.0	6.59	1.36	0.042	0.119
2.5	7.79	2.22	0.060	0.194
3.0	8.72	3.13	0.076	0.258
3.5	9.47	4.00	0.091	0.314
4.0	10.09	5.15	0.105	0.362
4.5	10.57	6.36	0.118	0.401
5.0	10.95	7.46	0.128	0.433
6.0	11.39	10.00	0.144	0.469
7.0	11.59	11.52	0.152	0.481
8.0	11.73	11.77	0.155	0.486
9.0	11.82	11.84	0.157	0.488
10.0	11.87	11.87	0.157	0.488
12.0	11.89	11.88	0.157	0.487
14.0	11.90	11.89	0.157	0.488
16.0	11.91	11.91	0.157	0.489
20.0	11.94	11.93	0.158	0.490
25.0	11.94	11.94	0.158	0.491
30.0	11.94	11.94	0.158	0.491
40.0	11.95	11.95	0.158	0.491
∞	11.95	11.95	0.158	0.491

† Normalized with respect to gust downwash angle.

* Normalized with respect to steady magnitude on the wing corresponding to gust.

Table 7

GROWTH OF LIFT FOR (1-COSINE) GUSTS OF INCLINATION $\psi = 40^{\circ}$

σ	L/L_0 for gust lengths $\sigma_g \bar{c}$					
	$\sigma_g = 0$	$\sigma_g = 2$	$\sigma_g = 5$	$\sigma_g = 10$	$\sigma_g = 20$	$\sigma_g = 35$
0.4	0.013	0.000	0.000	0.000	0.000	0.000
0.8	0.046	0.003	0.001	0.000	0.000	0.000
1.2	0.095	0.014	0.003	0.001	0.000	0.000
1.6	0.158	0.038	0.007	0.002	0.000	0.000
2.0	0.228	0.077	0.017	0.004	0.001	0.000
2.5	0.307	0.146	0.037	0.010	0.003	0.001
3.0	0.380	0.225	0.069	0.019	0.005	0.002
3.5	0.447	0.304	0.112	0.032	0.008	0.003
4.0	0.516	0.378	0.167	0.050	0.013	0.004
4.5	0.582	0.448	0.230	0.073	0.019	0.006
5.0	0.643	0.515	0.299	0.102	0.027	0.009
6.0	0.760	0.642	0.442	0.175	0.049	0.016
7.0	0.844	0.756	0.574	0.268	0.079	0.027
8.0	0.888	0.840	0.691	0.376	0.117	0.040
9.0	0.916	0.887	0.785	0.490	0.163	0.057
10.0	0.937	0.916	0.853	0.602	0.216	0.077
12.0	0.963	0.951	0.923	0.780	0.340	0.126
14.0	0.977	0.971	0.956	0.888	0.478	0.186
16.0	0.985	0.982	0.973	0.941	0.617	0.256
18.0	0.990	0.988	0.983	0.966	0.744	0.334
20.0	0.993	0.992	0.989	0.979	0.846	0.417
24.0	0.996	0.995	0.994	0.991	0.954	0.588
28.0	0.997	0.997	0.997	0.995	0.984	0.747
32.0	0.998	0.998	0.998	0.997	0.993	0.875
36.0	0.999	0.999	0.998	0.998	0.996	0.955
40.0	0.999	0.999	0.999	0.999	0.998	0.985
50.0	0.999	0.999	0.999	0.999	0.999	0.998
60.0	1.000	1.000	1.000	1.000	0.999	0.999

Table 8

REQUIRED AILERON ANGLES, TAILPLANE LIFT AND RESIDUAL ROOT BENDING MOMENT TO NEUTRALIZE AN INCLINED (1-COSINE) DOWN-GUST

$M = 0.8$, $\sigma_g = 10$, $\psi = 40^\circ$, tailplane lift at $x_T/\bar{c} = 3$

σ	Control angles†		Tailplane lift*	Bending moment*
	Leading side δ_ℓ	Trailing side δ_t		
0.0	0.00	0.00	-0.000	0.000
0.4	0.00	0.00	-0.000	0.000
0.8	0.01	0.00	-0.000	0.000
1.2	0.03	0.01	-0.000	0.000
1.6	0.10	0.02	-0.001	0.002
2.0	0.22	0.06	-0.001	0.005
2.5	0.47	0.15	-0.004	0.014
3.0	0.87	0.33	-0.008	0.029
3.5	1.41	0.60	-0.014	0.054
4.0	2.11	0.98	-0.023	0.089
4.5	2.96	1.47	-0.034	0.135
5.0	3.96	2.10	-0.047	0.192
6.0	6.32	3.76	-0.082	0.337
7.0	9.01	5.92	-0.125	0.517
8.0	11.78	8.45	-0.172	0.715
9.0	14.33	11.10	-0.219	0.911
10.0	16.43	13.61	-0.261	1.086
12.0	18.67	17.26	-0.316	1.309
14.0	19.13	18.81	-0.333	1.372
16.0	19.01	19.00	-0.333	1.366
18.0	18.88	18.87	-0.330	1.354
22.0	18.85	18.85	-0.329	1.352
26.0	18.88	18.87	-0.329	1.354
30.0	18.87	18.87	-0.329	1.354
40.0	18.87	18.87	-0.329	1.353
∞	18.86	18.86	-0.329	1.353

† Normalized with respect to gust downwash angle.

* Normalized with respect to steady magnitude on the wing corresponding to the gust.

LIST OF SYMBOLS

B	instantaneous bending moment
B_0	steady bending moment in second of equations (3-23)
B_ℓ, B_t	bending moment on leading, trailing side of wing in equations (2-12) to (2-14)
B_{max}	maximum bending moment
$\bar{c}$	mean chord of wing
i	$\sqrt{-1}$; integer or subscript denoting force mode
j	integer or subscript denoting upwash mode
$K_i(\sigma)$	Küssner function for mode i in equations (2-28) and (2-29)
$K_T(\sigma)$	Küssner function for moment about $x = x_T$ in equation (3-17)
ℓ_g	non-dimensional loading due to step gust
ℓ_j	non-dimensional complex loading in expression (2-6)
ℓ_x, ℓ_y	wavelength of gust in streamwise, spanwise direction
L	instantaneous lift force
L_0	steady lift force in first of equations (3-23)
L_C, L_T	lift force at location of canard, tailplane
$\mathcal{L}$	instantaneous rolling moment
$\mathcal{L}(\sigma,\sigma_g)$	$\mathcal{L}$ for (1-cosine) gust in equation (4-4)
$\mathcal{L}_{max}$	maximum rolling moment
m	number of spanwise terms
M	Mach number of stream
N	number of chordwise terms
q_i	integers ($i = 1,2,\ldots,N$) (see Ref 7)
$q_j(\tau)$	generalized coordinate in mode j in equations (3-2) and (3-3)
$q_j^{(n)}(\tau)$	approximation to $q_j(\tau)$ after nth iteration
$Q_{T3}(\bar{\nu})$	generalized force indicated in equations (3-20)
$Q_{Tg}(\infty)$	steady generalized force in second of equations (3-20)
$Q_i(\tau)$	force coefficient in mode i in equation (3-4)
$Q_{ig}(\sigma)$	generalized force due to step gust in equation (2-25)
$Q_{ij}(\bar{\nu})$	complex generalized force in equation (2-7), $Q'_{ij}(\bar{\nu}) + i\bar{\nu}Q''_{ij}(\bar{\nu})$
$\mathcal{R}$	real part of
s	semi-span of wing

LIST OF SYMBOLS (continued)

t	time measured from entry of wing into gust
t_0	time when wing root leading edge enters gust
U	speed of stream
w	upwash in equation (2-1), (2-5) or (4-1)
w_j	upwash in mode j (= 1 to 5) in equations (2-8) to (2-10) and (2-2)
$W_{T3}(\sigma)$	Wagner function for moment about $x = x_T$ in equation (3-18)
$W_{ij}(\sigma)$	Wagner function in equation (3-1)
x	streamwise coordinate relative to pitching axis in Fig 1
$\bar{x}$	streamwise centre of pressure
$x_0(\psi)$	location of gust front on centre-line at $t = 0$ in equation (2-23)
x_a	general pitching axis
x_C, x_T	location of canard lift, tailplane lift
x_g	length of (1-cosine) gust
$x_h(y)$	location of aileron hinge in Fig 1
y	spanwise coordinate relative to centre-line
z	upward coordinate
z_i	displacement in mode i (= 1 to 5) in equations (2-8), (2-10) and (2-11)
α	local incidence of (1-cosine) gust in equation (4-5)
α_g	final incidence of gust
δ	instantaneous aileron angle in streamwise plane (radians)
δ_ℓ, δ_t	aileron angles on leading, trailing side of wing
δ_{max}	maximum aileron angle
$\dot{\delta}_{max}$	non-dimensional maximum aileron rate in equation (3-27)
$\bar{\eta}$	spanwise centre of pressure in terms of y/s
Λ_ℓ	angle of sweepback of leading edge of wing
$\bar{\nu}$	frequency parameter, $\omega\bar{c}/U$
ρ	density of stream
σ	distance of travel in mean chords, $Ut/\bar{c}$
σ_0	σ relative to entry of root leading edge, $U(t - t_0)/\bar{c}$
σ_e	σ_0 as wing enters gust in equation (2-21)
σ_f	σ_0 as wing becomes fully immersed (see Fig 1)

LIST OF SYMBOLS (concluded)

σ_g non-dimensional gust length, $x_g/\bar{c}$

σ_m the lesser of σ and σ_g

τ non-dimensional time, $Ut/\bar{c}$

ψ angle of inclination of gust front in Fig 1

ω circular frequency

REFERENCES

No.	Author	Title, etc
1	H.C. Garner	The application of subsonic theoretical aerodynamics to active controls. RAE Technical Report 81060 (1981)
2	H. Lomax	Indicial aerodynamics. AGARD Manual on Aeroelasticity, Vol.II, Chapter 6 (1960)
3	H. Wagner	Über die Entstehung des dynamischen Auftriebes von Tragflügeln. ZAMM, Vol.5, No.1, pp.17-35 (1925)
4	H.G. Küssner	Zusammenfassender Bericht über den instationären Auftrieb von Flügeln. Luftfahrtforschung, Vol.13, pp.410-424 (1936)
5	H.C. Garner	The calculated growth of lift and moment on a swept wing entering a discrete vertical gust at subsonic speeds. RAE Technical Report 72010 (ARC CP 1241) (1972)
6	H. Ashley G. Zartarian	Piston theory - A new aerodynamic tool for the aeroelastician. J. Aeronaut. Sci., Vol.23, pp.1109-1118 (1956)
7	D.E. Davies	Theoretical determination of subsonic oscillatory airforce coefficients. RAE Technical Report 76059 (ARC R&M 3804) (1976)
8	H.C. Garner	A phenomenon of subsonic aerodynamic loading from rapid aileron oscillations. RAE Technical Report 80025 (1980) Proceedings of the Colloquium honoring Hans Georg Küssner on the occasion of his 80th birthday, Göttingen, September 24, 1980
9	H.C. Garner	On the application of subsonic wing theory to edge forces and roll-rate derivatives. RAE Technical Report 73030 (ARC R&M 3758, Part II) (1973)

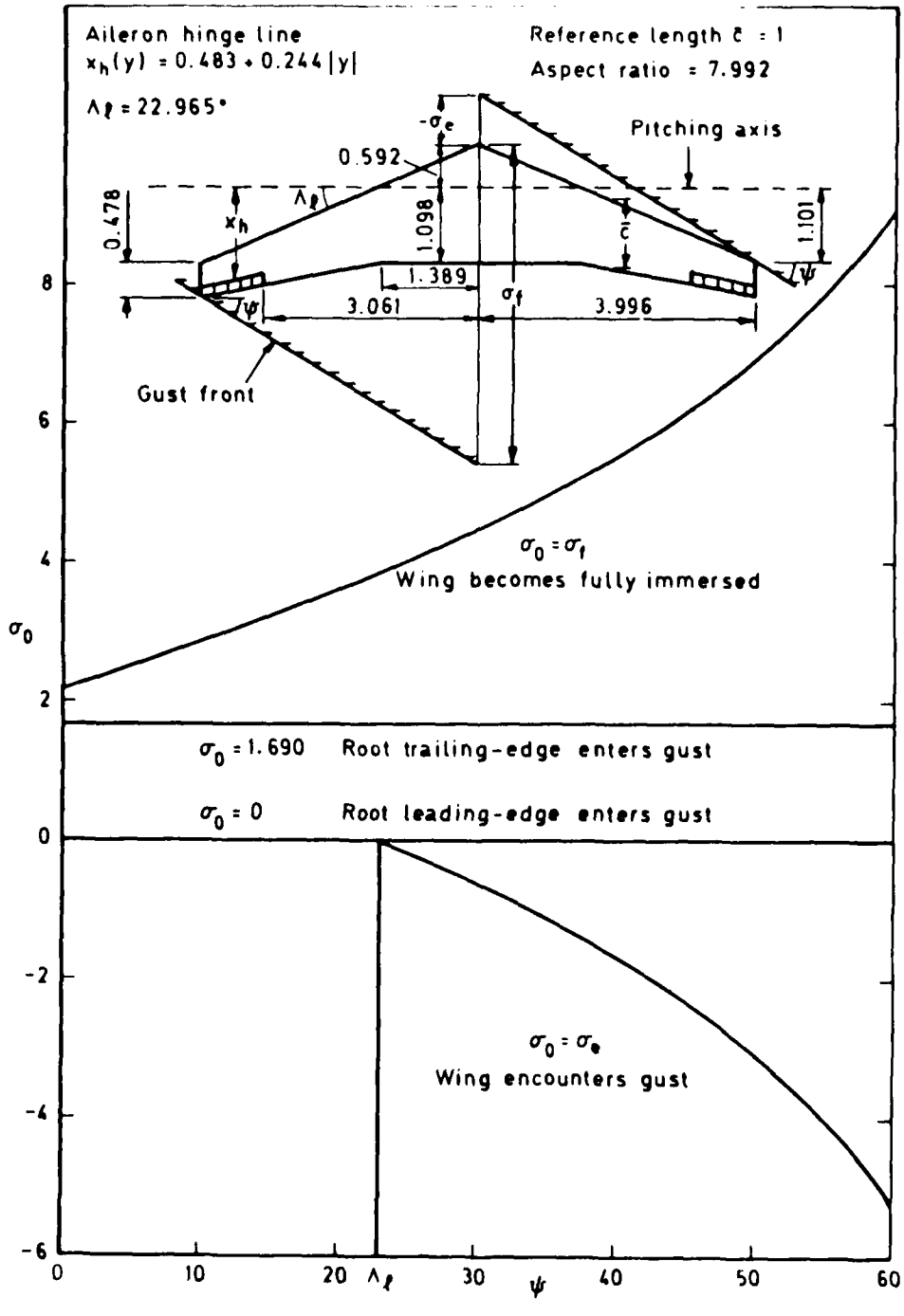

Fig 1 Planform with 25% chord ailerons in inclined step gust

Fig 2

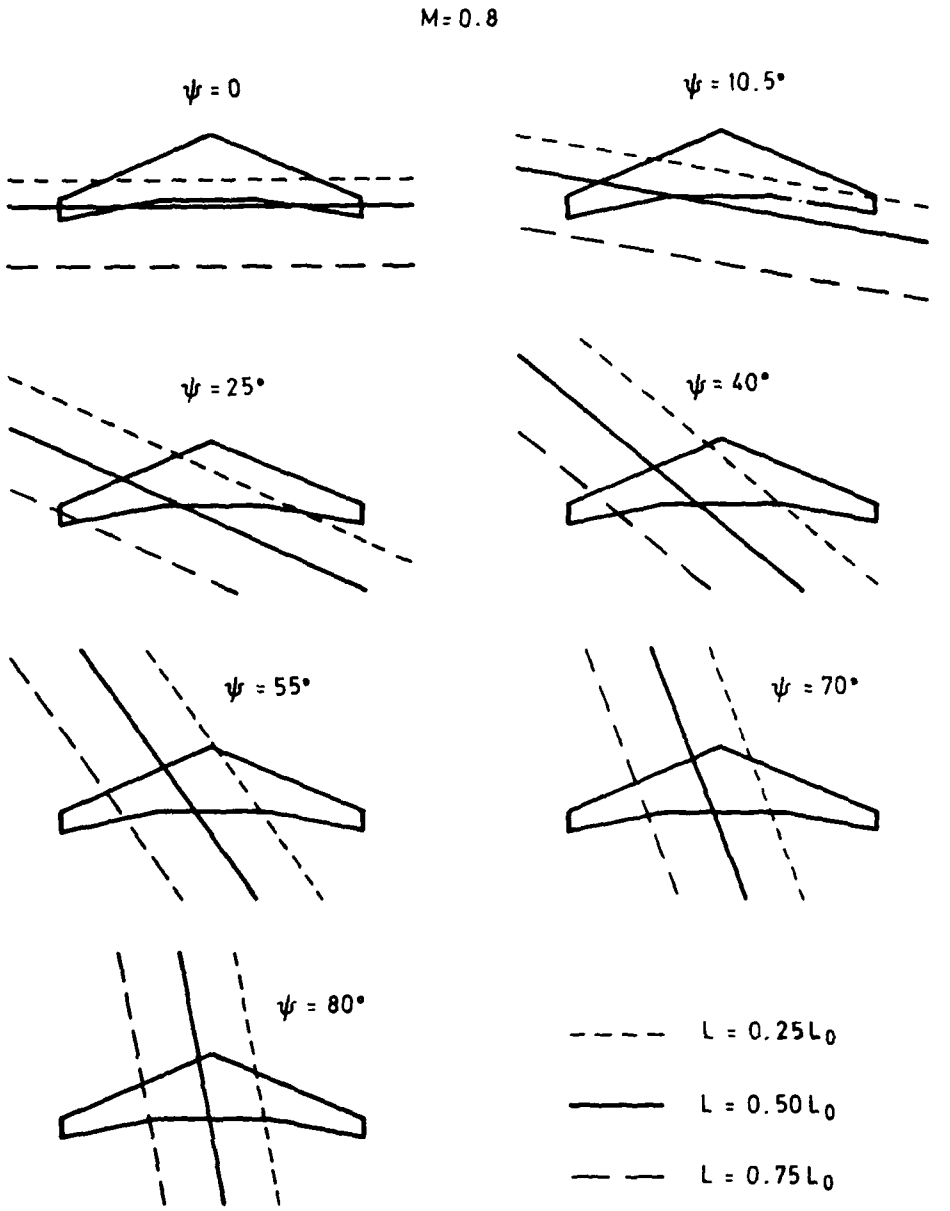

Fig 2 Position of gust front at various inclinations for equal steps in growth of lift

TR 81157

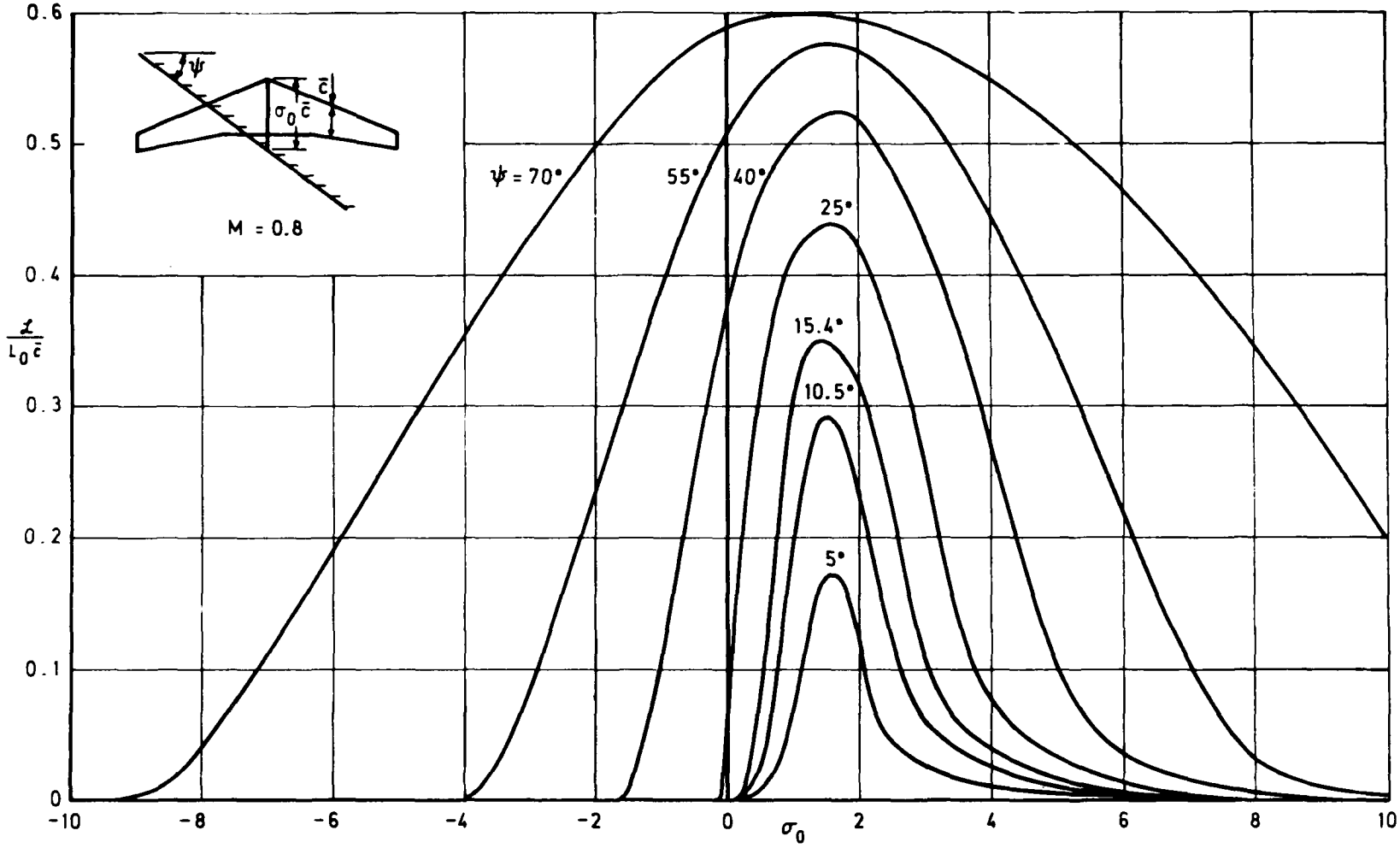

Fig 3 Transient rolling moment due to asymmetric entry into a step gust

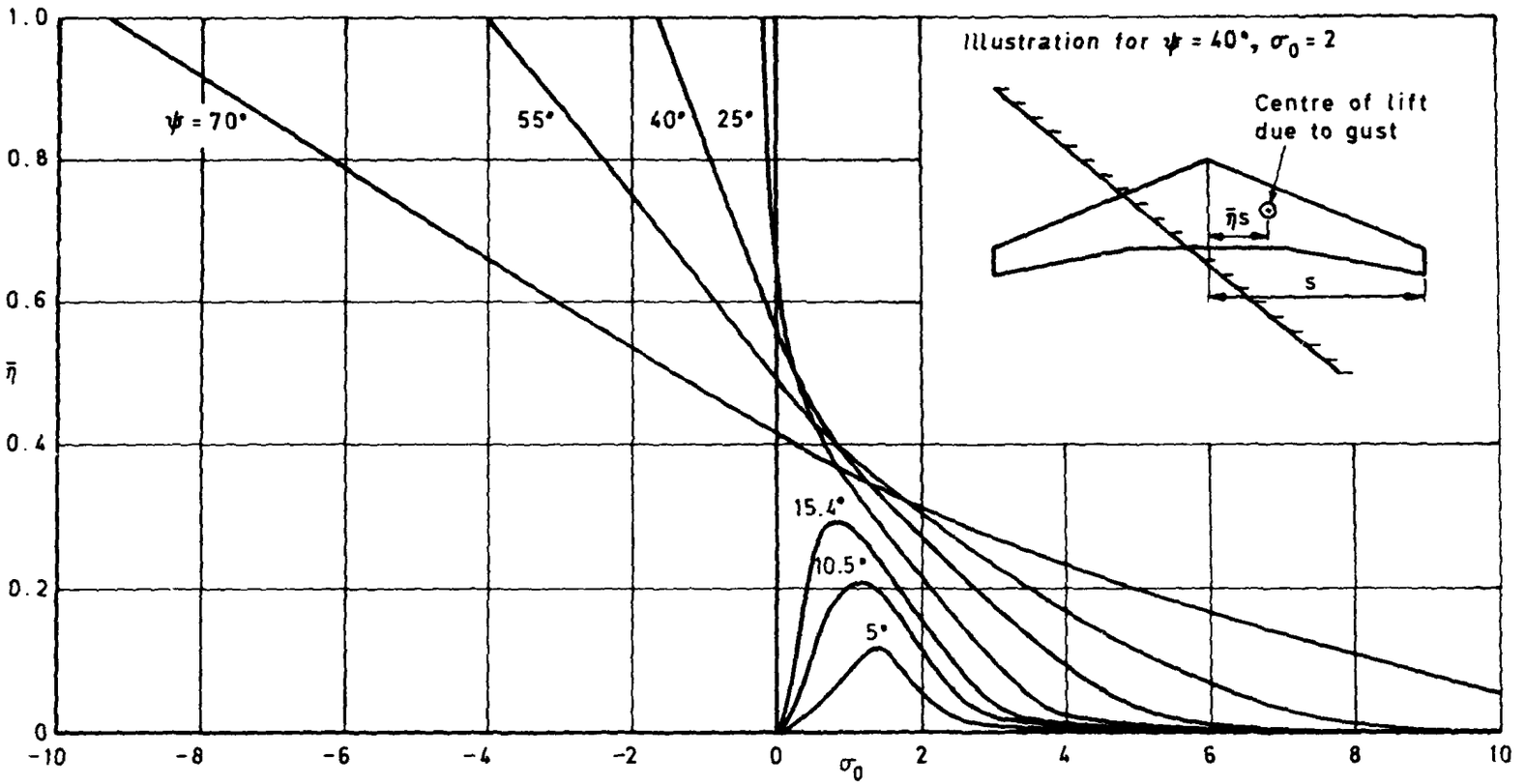

Fig 4 Spanwise centre of pressure due to asymmetric entry into a step gust (M = 0.8)

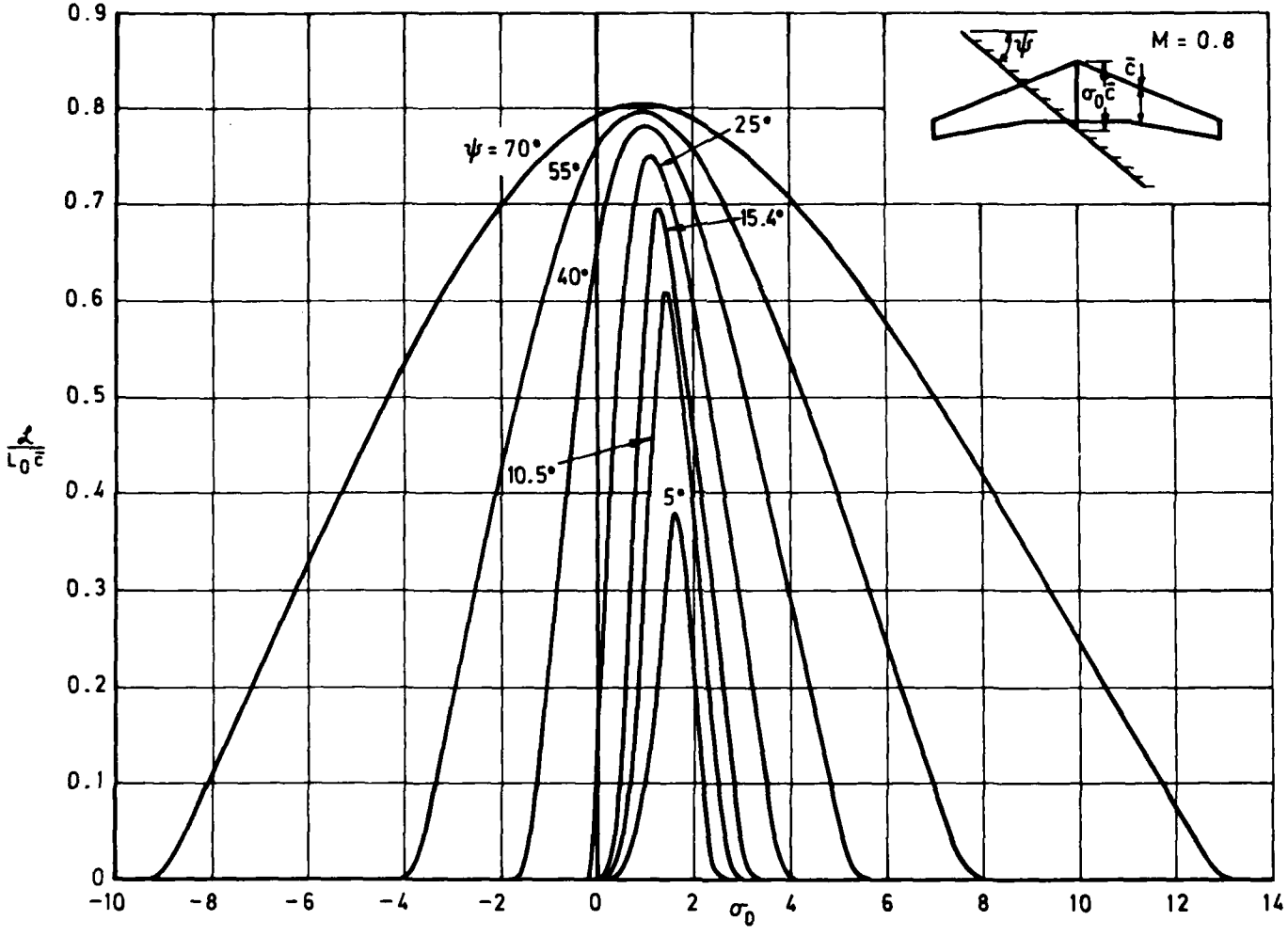

Fig 5 *Transient rolling moment from piston theory for asymmetric entry into a step gust*

Fig 6

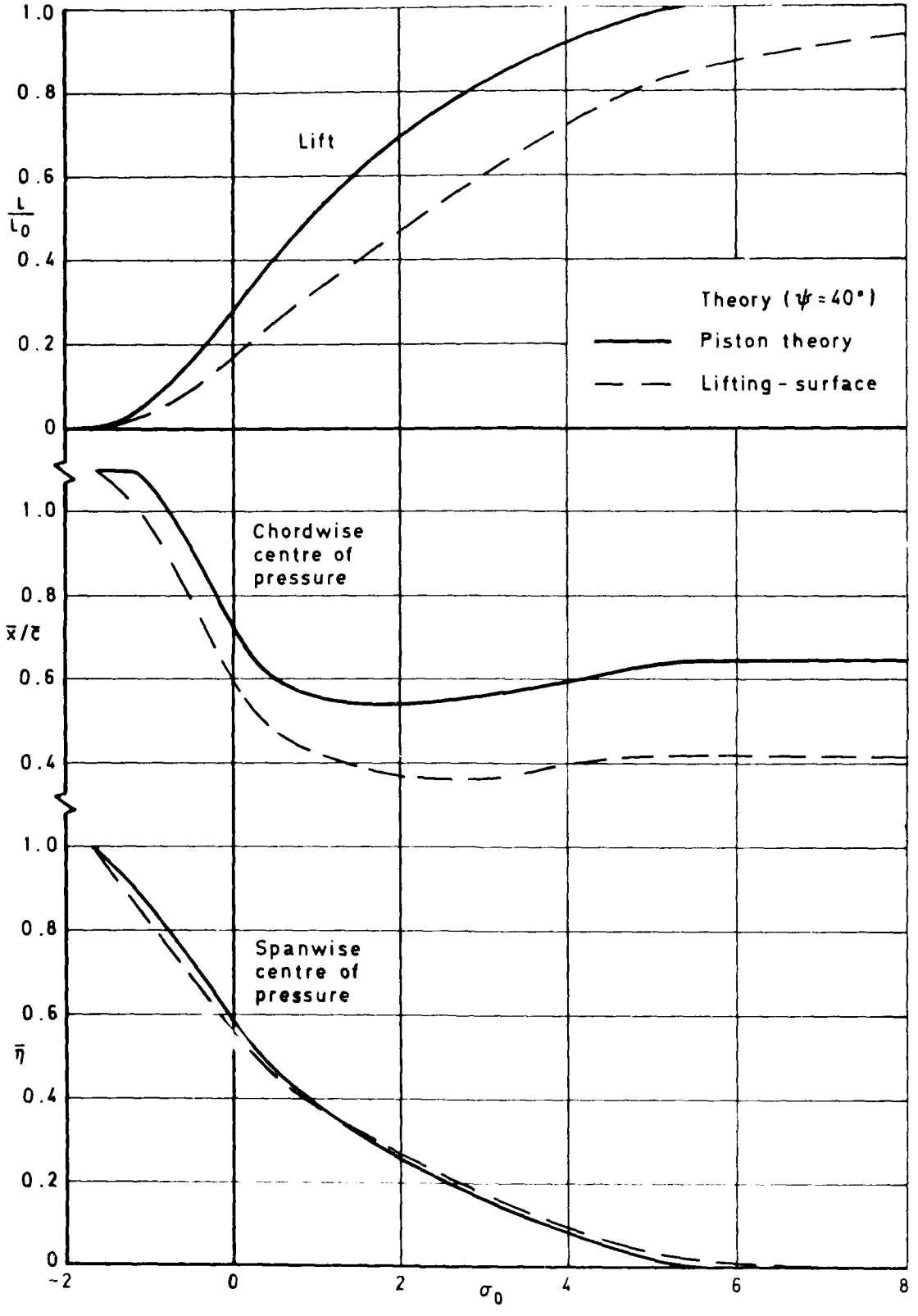

TR 81157

Fig 6 Comparison between piston and lifting-surface theories for step gust aerodynamics

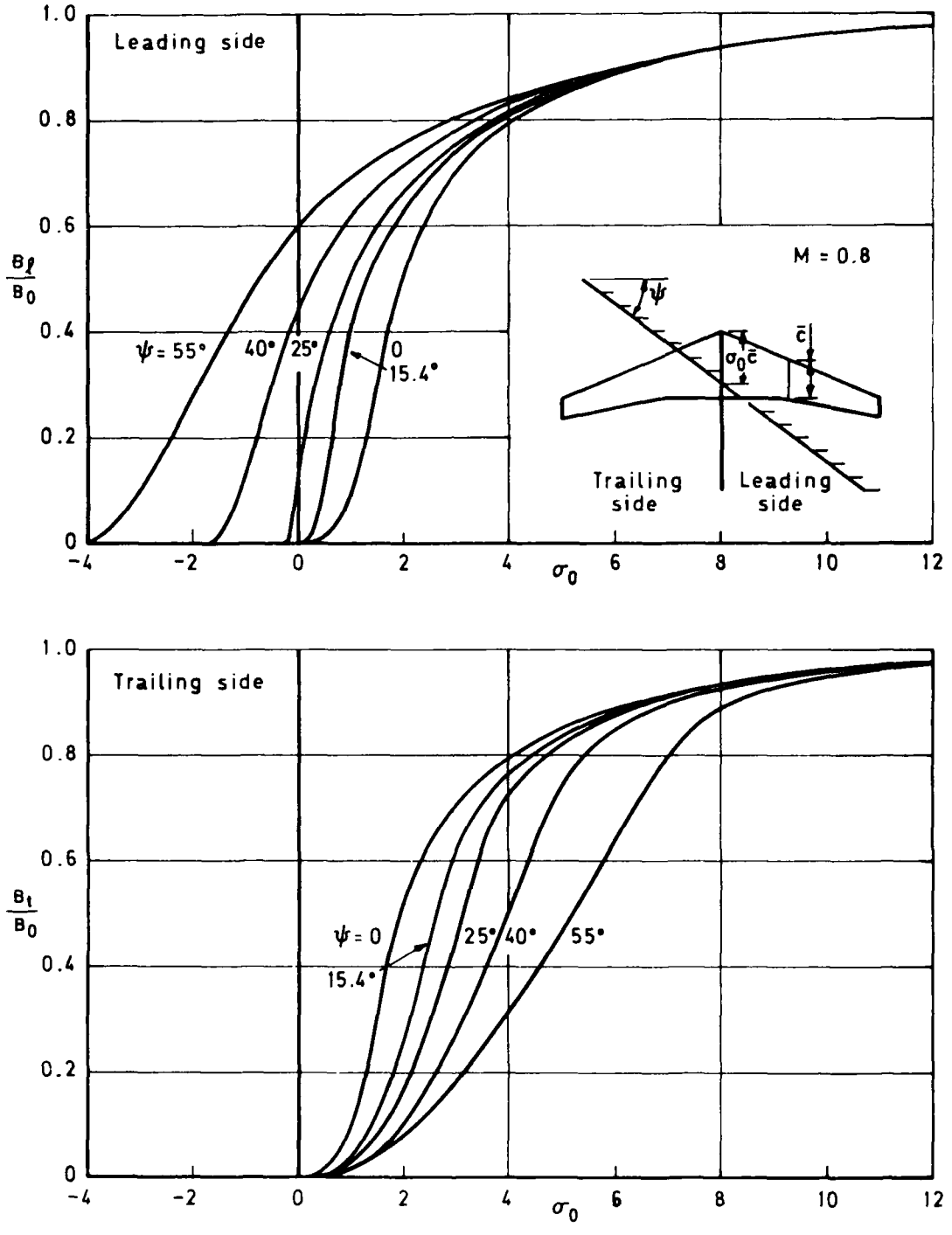

Fig 7 Normalized half-wing bending moments due to asymmetric entry into a step gust

Fig 8

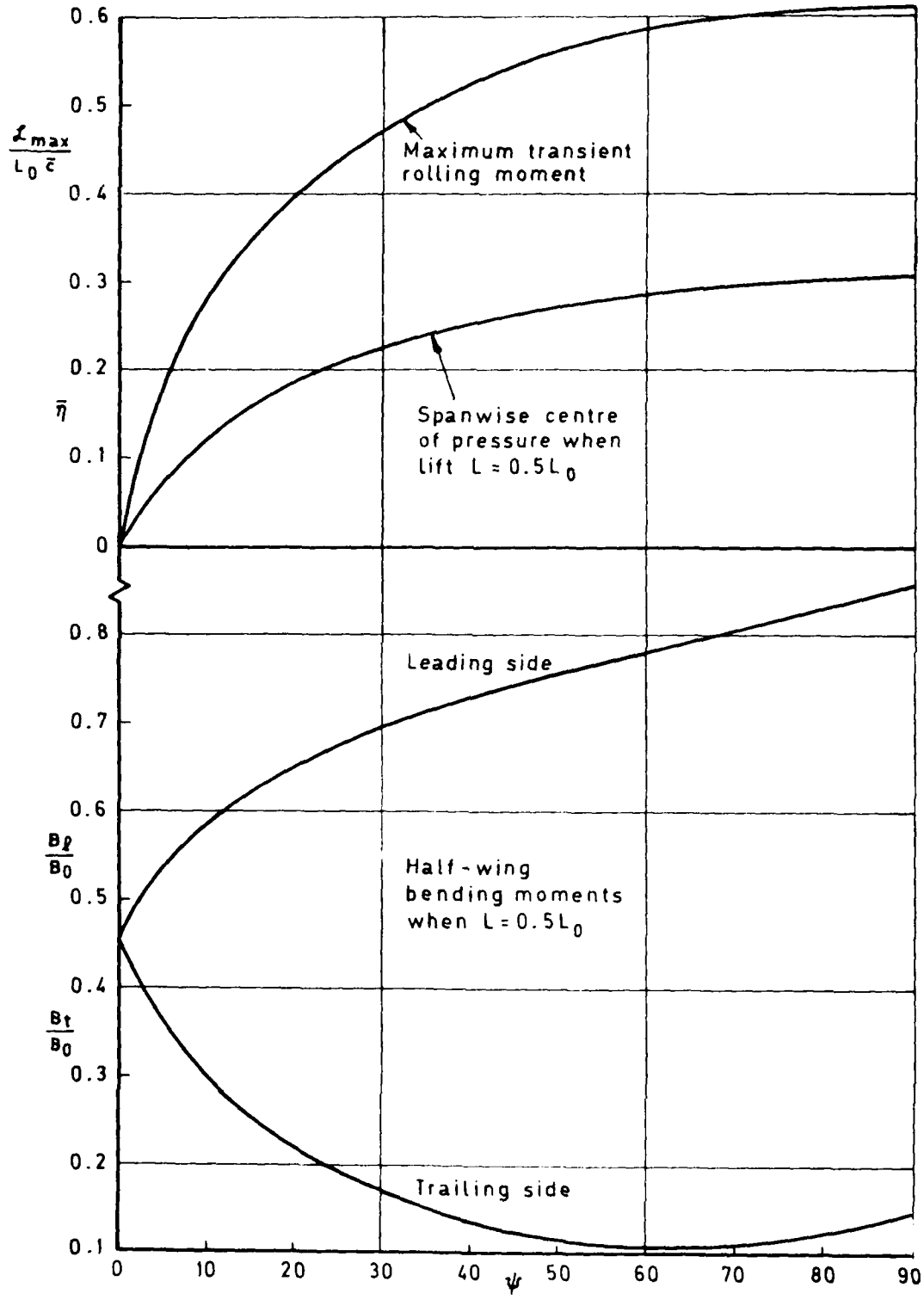

Fig 8 Influence of inclination of gust front on various force characteristics

TR 81157

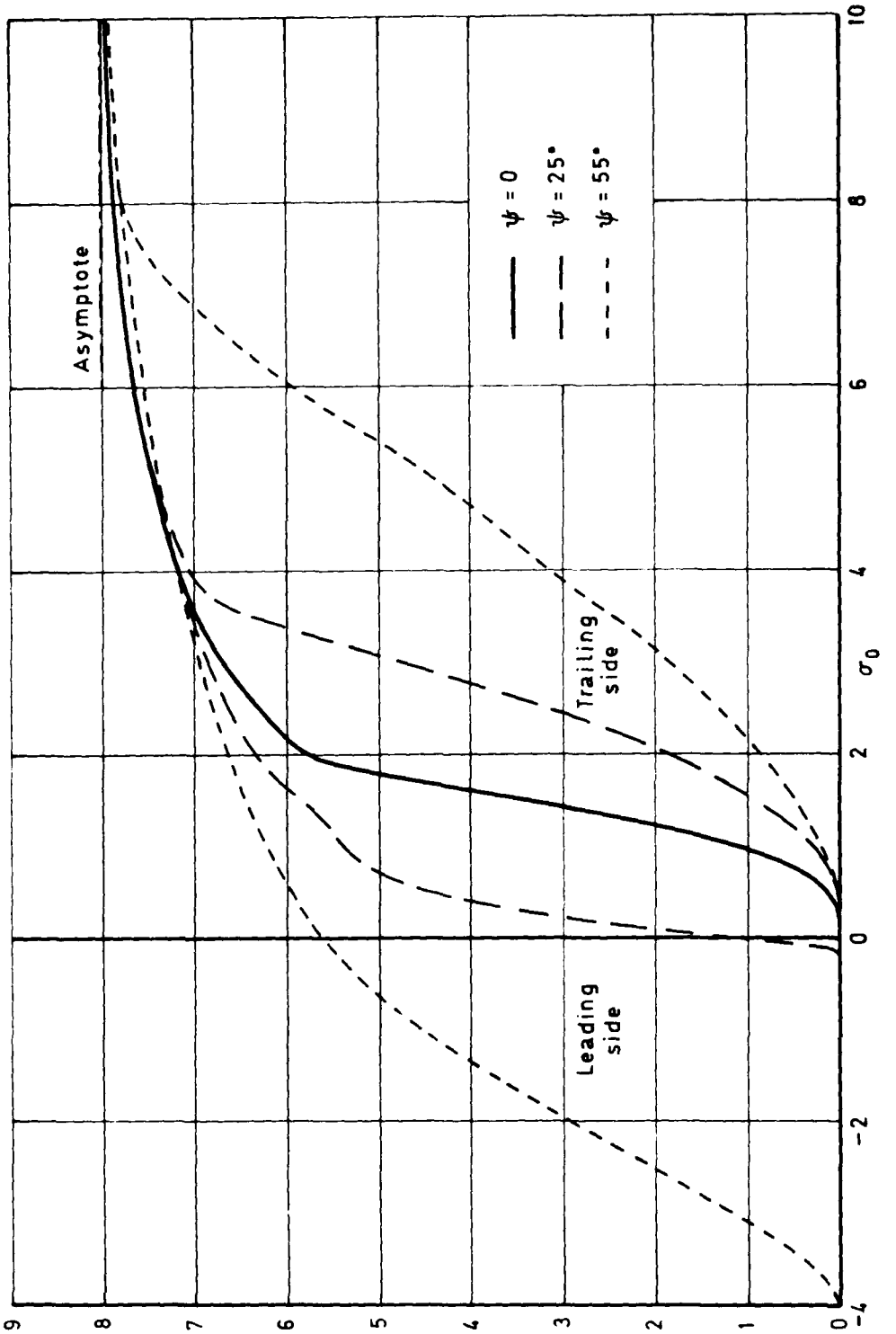

Fig 9 Control motions to neutralize bending and rolling moments due to step gusts

Fig 10

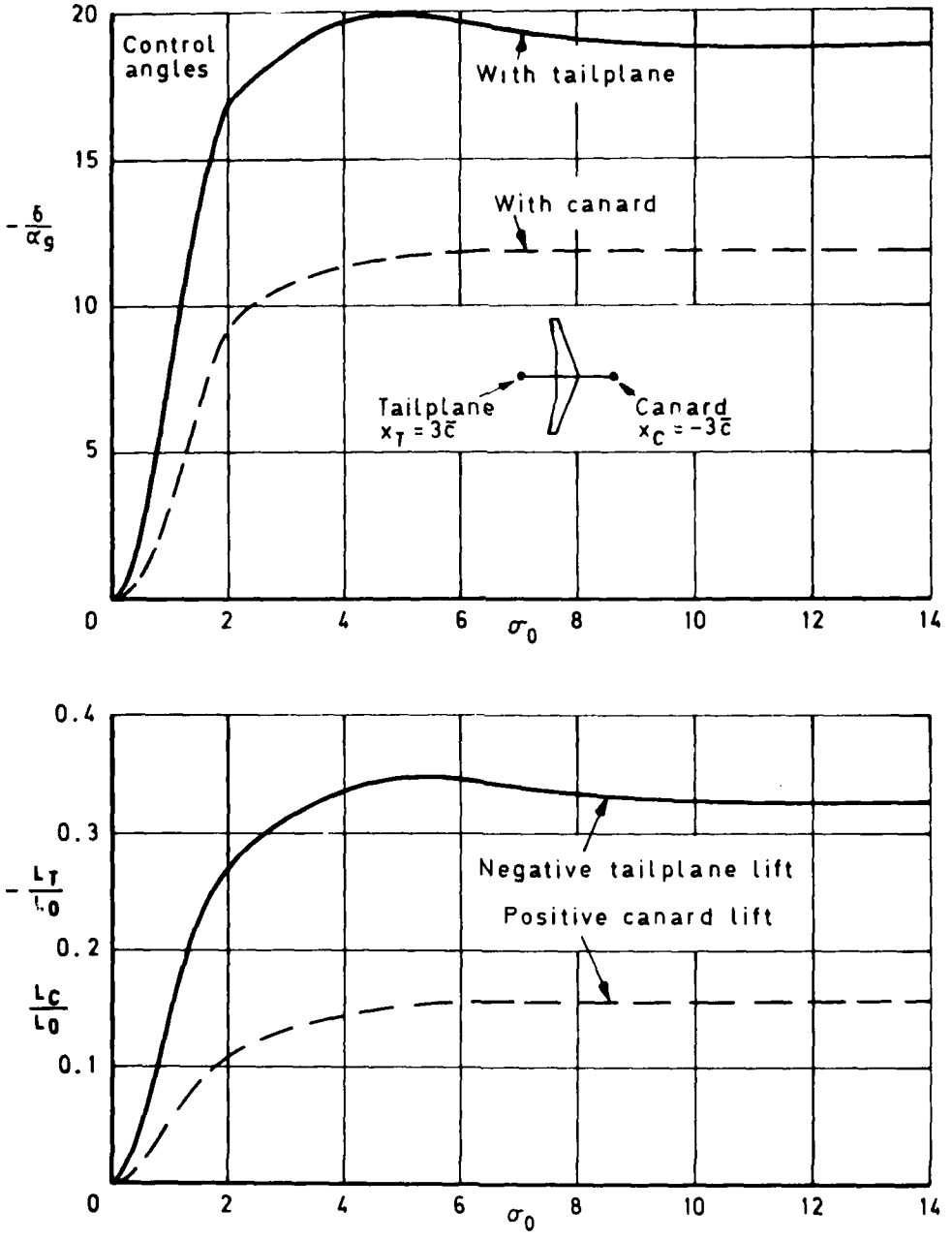

Fig 10 **Control angles and tailplane or canard lift to neutralize wing forces due to symmetric gust entry**

TR 81157

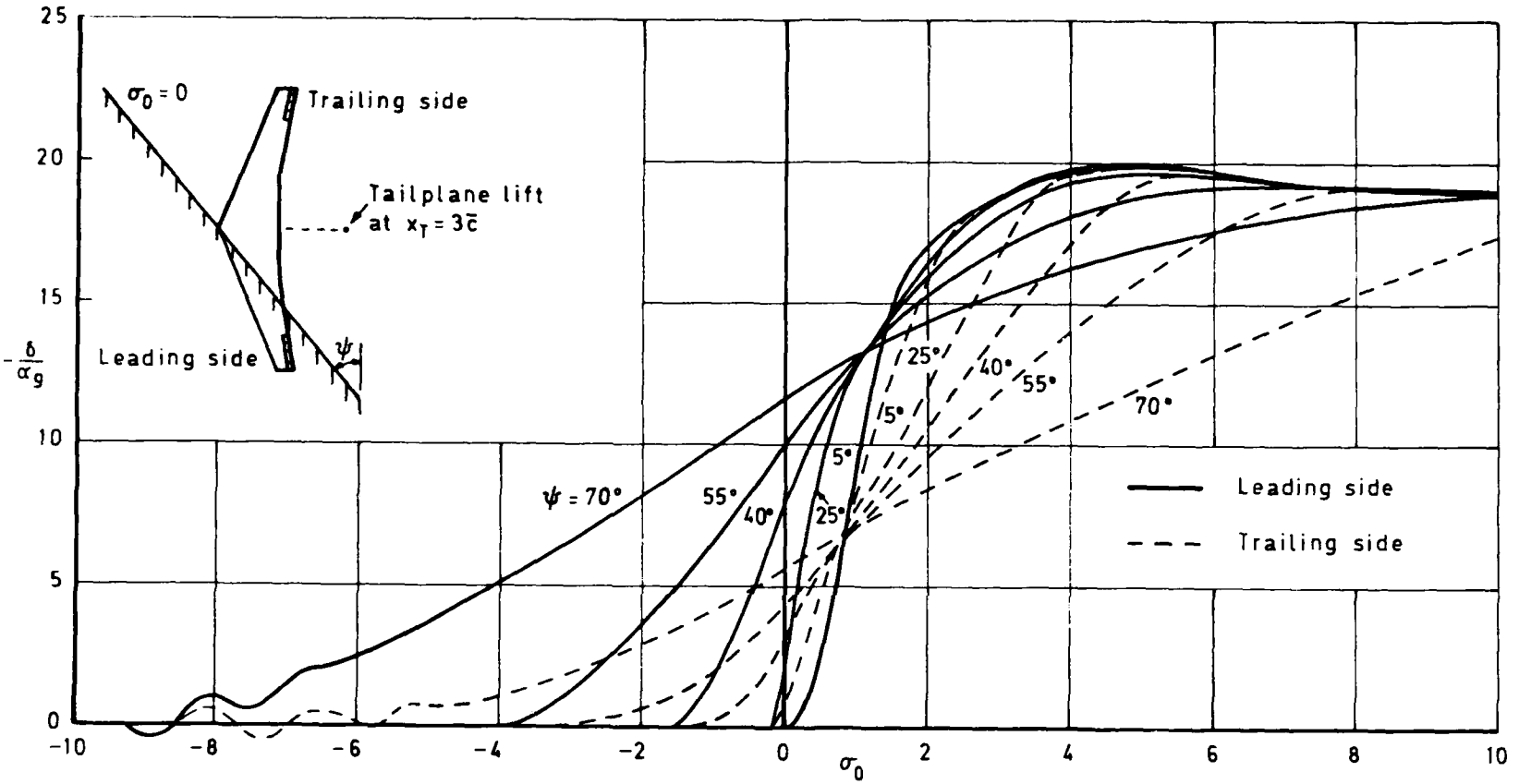

Fig 11 Control angles with tailplane lift to neutralize wing forces due to asymmetric gust entry

Fig 12

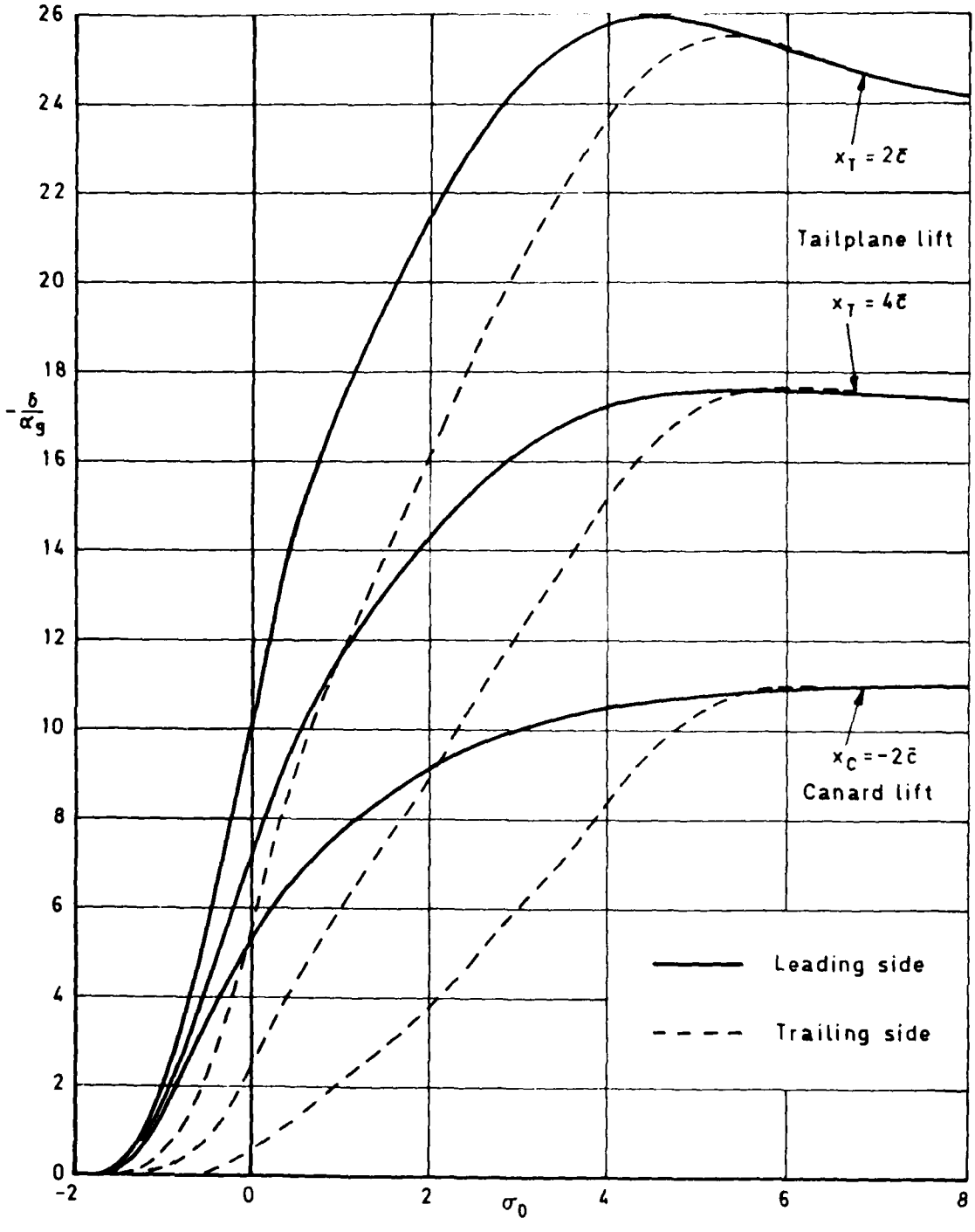

Fig 12 Asymmetric control angles with various locations of auxiliary lift to neutralize gust forces (ψ = 40°)

TR 81157

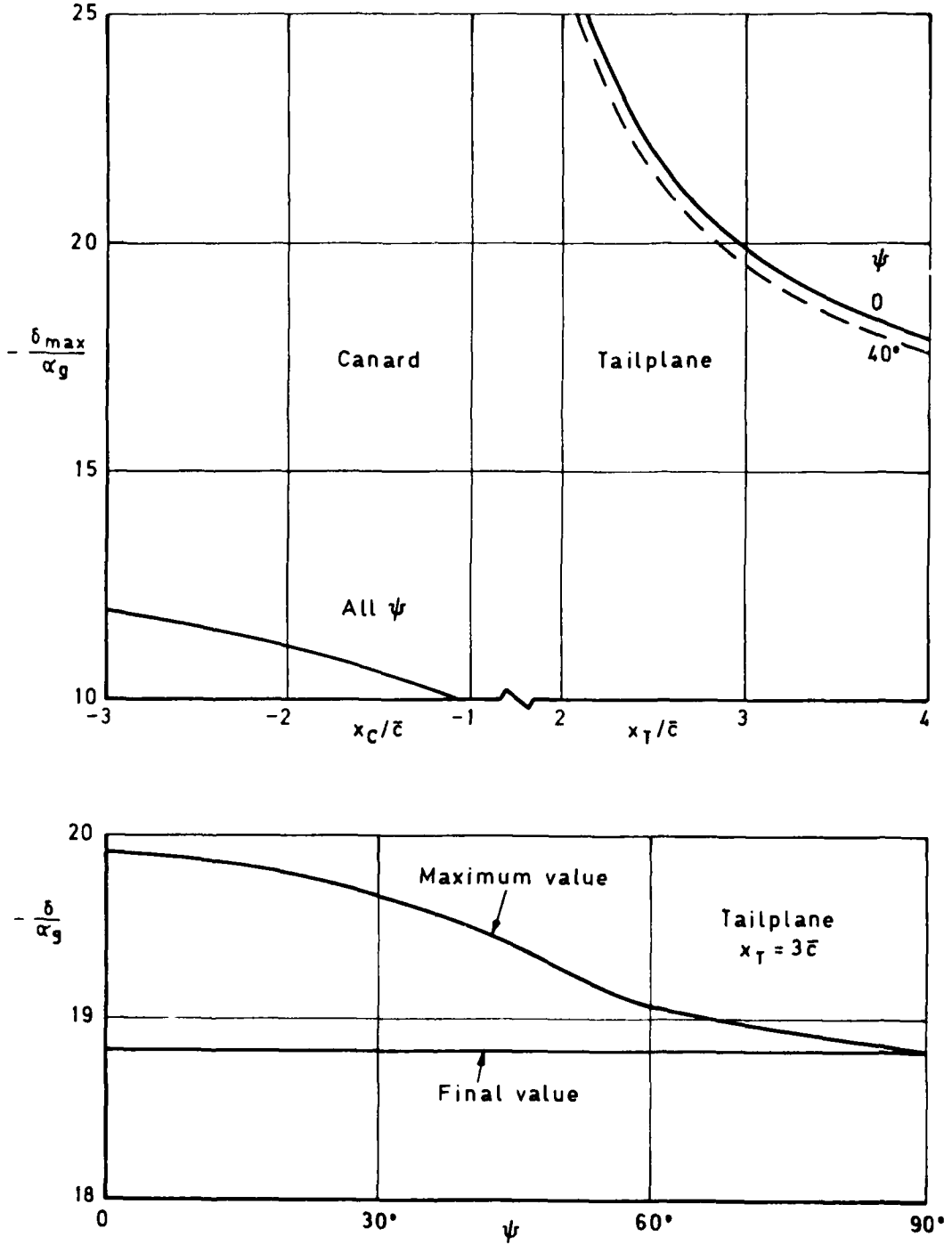

Fig 13 Maximum control angles with tailplane or canard lift to neutralize wing forces due to asymmetric gust entry

TR 81157

Fig 14

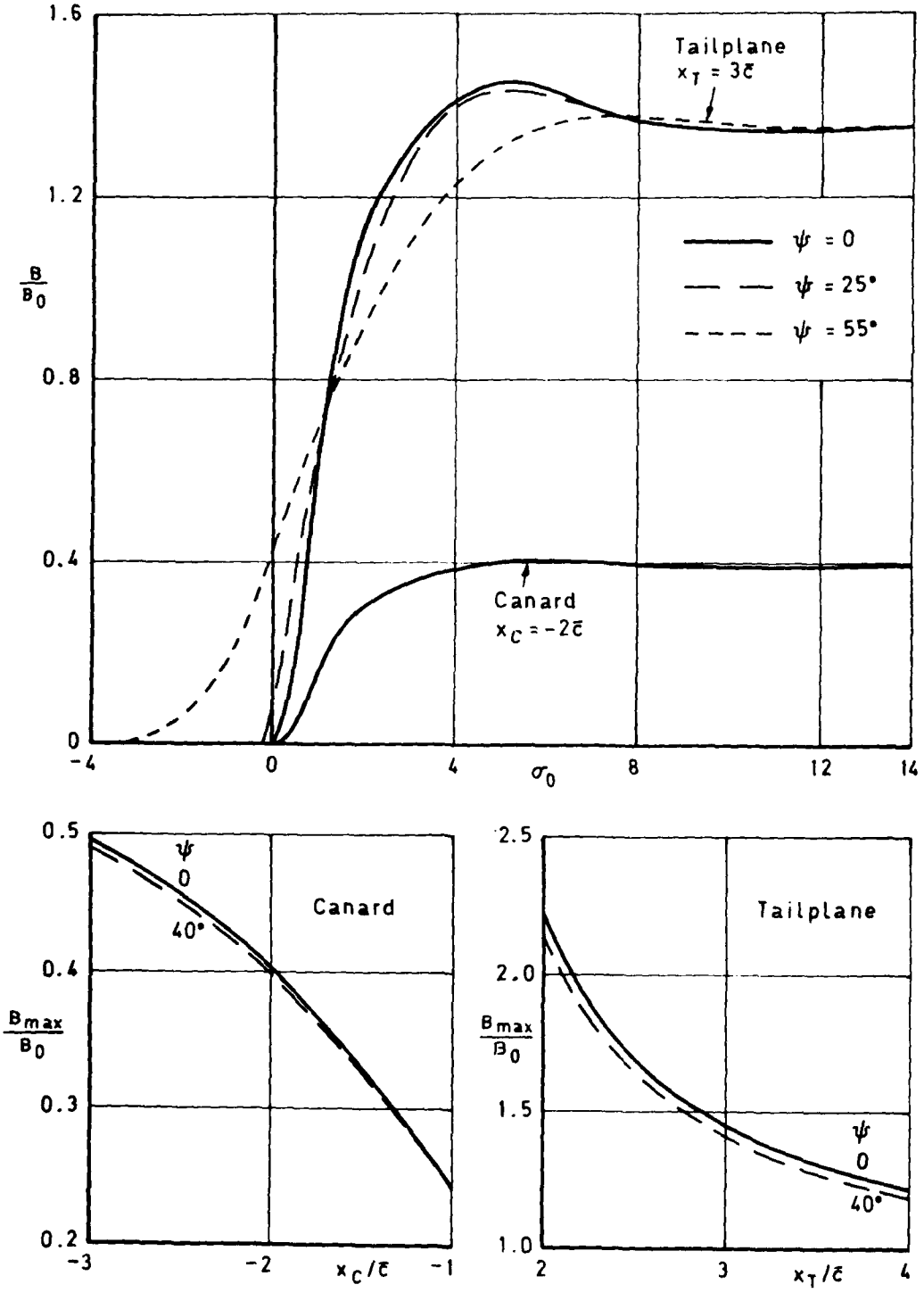

Fig 14 Bending moments with ailerons and tailplane or canard to neutralize wing forces due to gusts of various inclinations

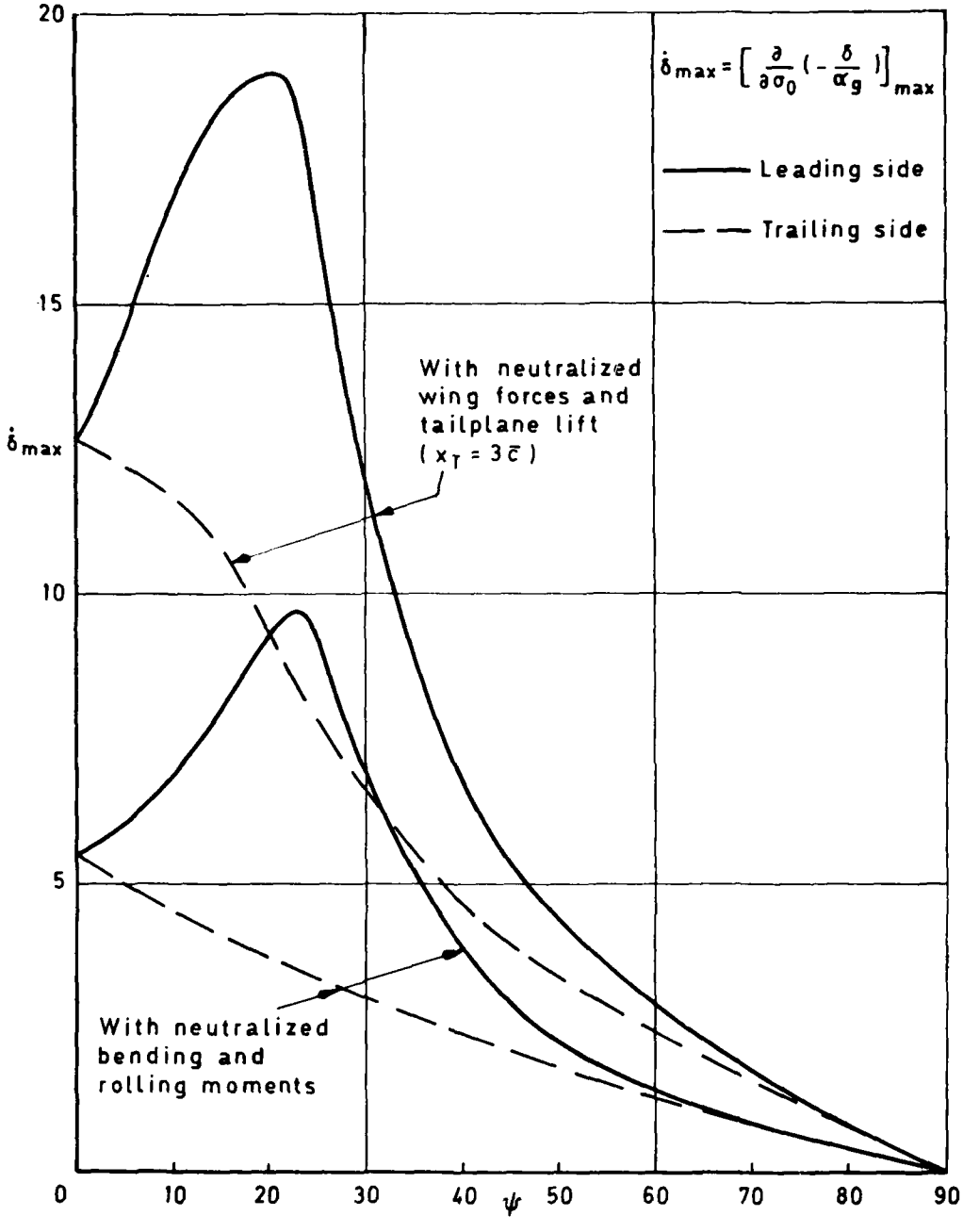

Fig 15 Influence of gust inclination on maximum control rates

Fig 16

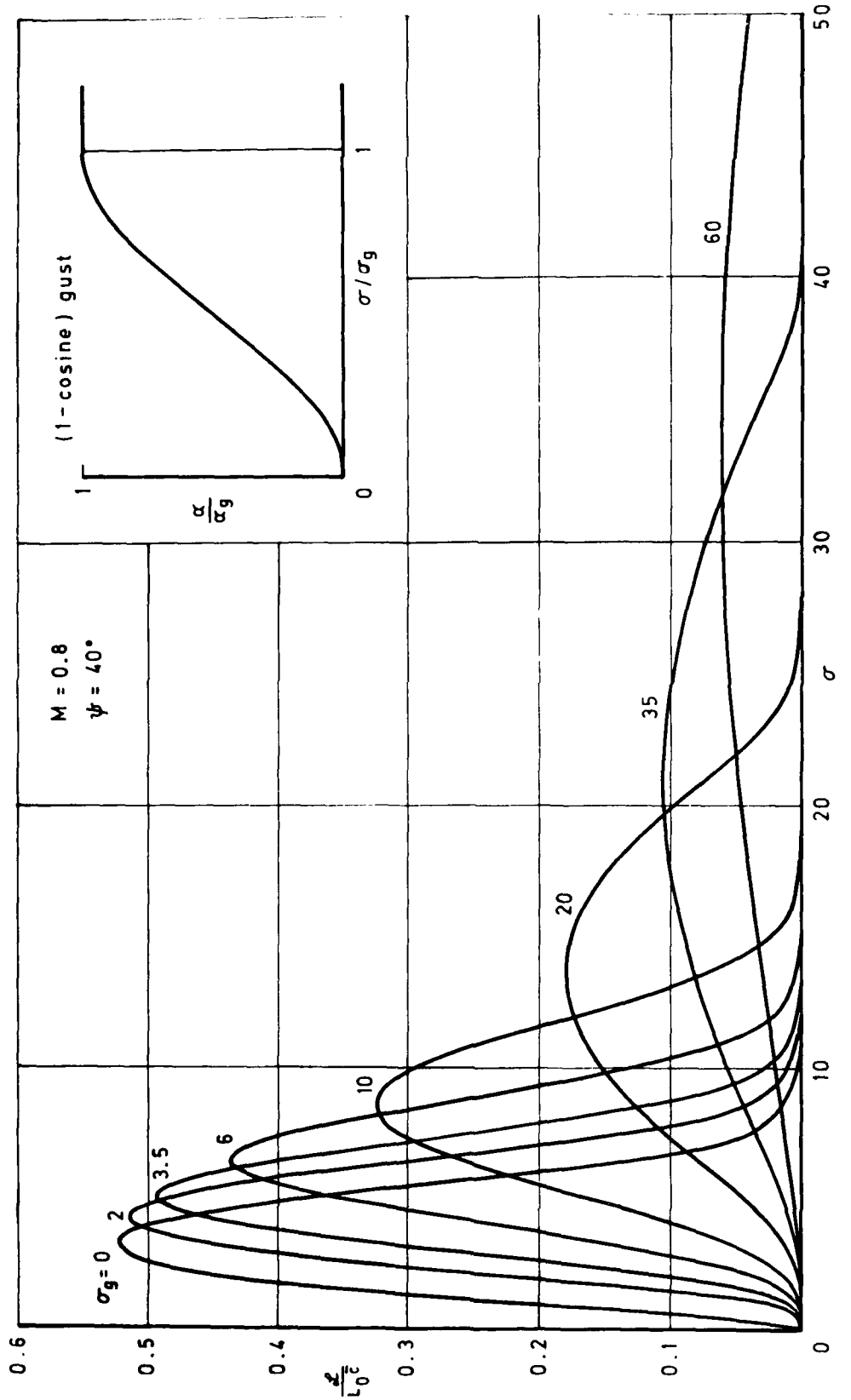

Fig 16 Influence of gust length on transient rolling moment due to asymmetric entry

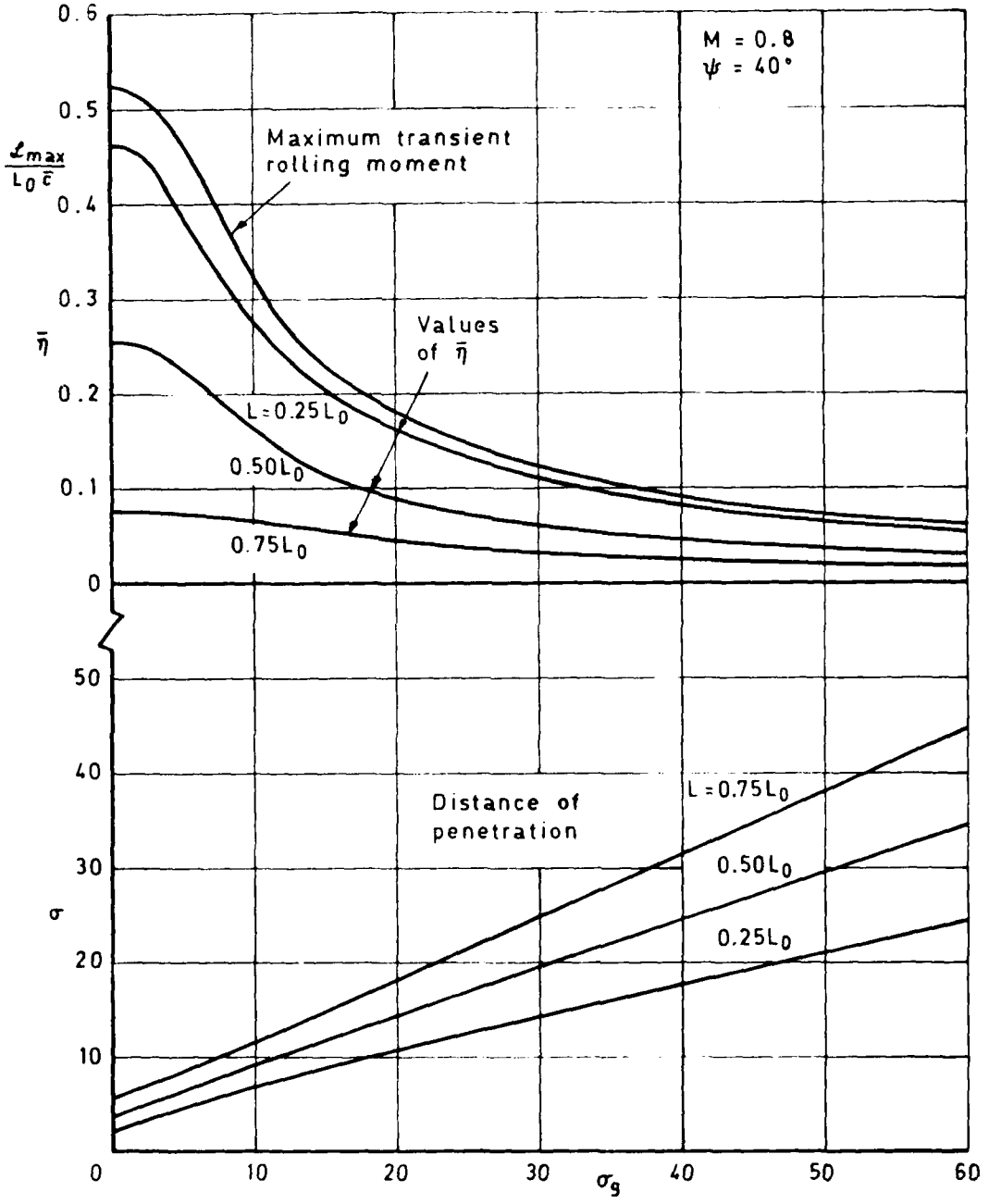

Fig 17 Influence of gust length on various force characteristics

Fig 18

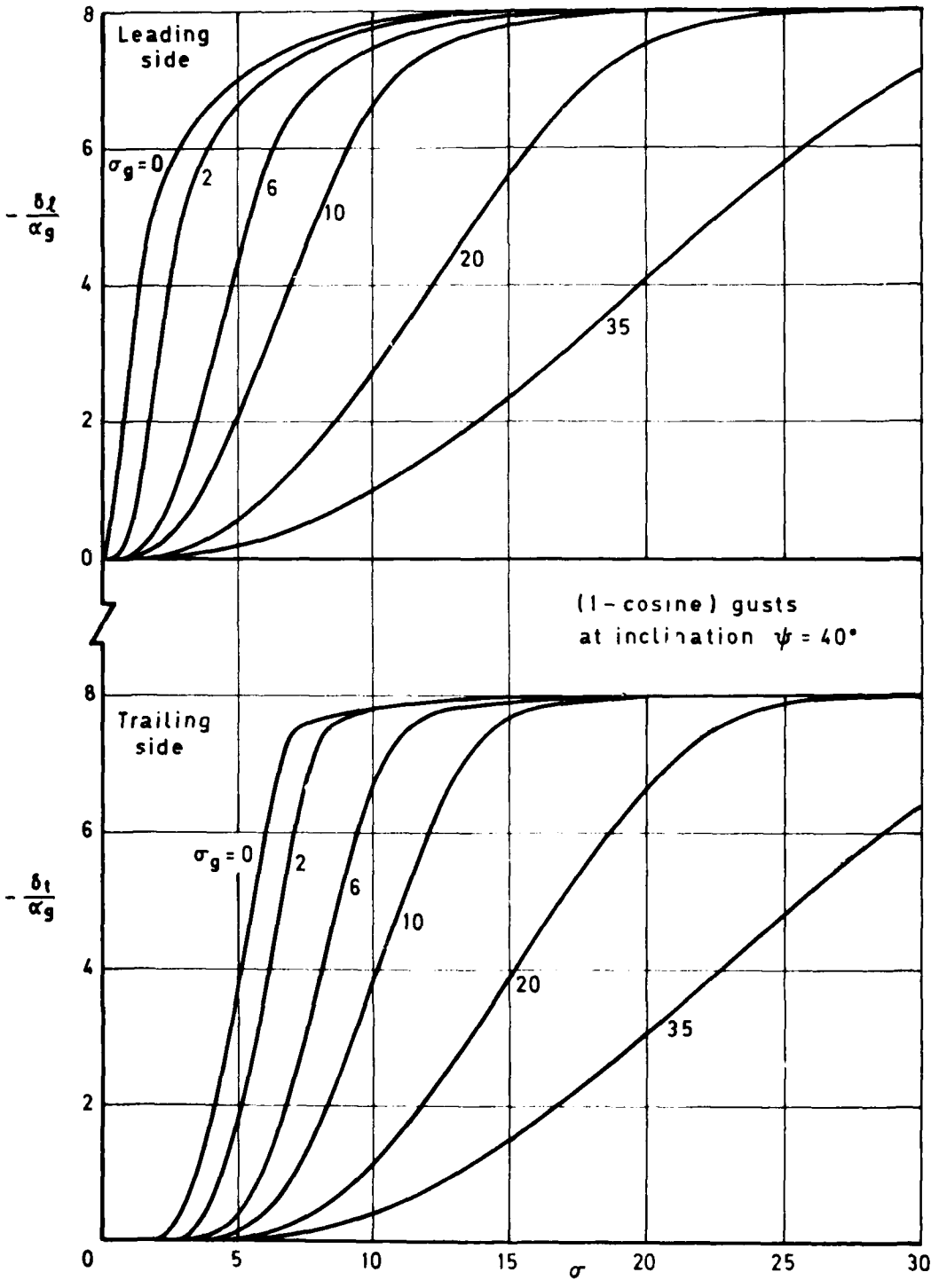

Fig 18 Influence of gust length on control motions to neutralize bending and rolling moments

TR 81157

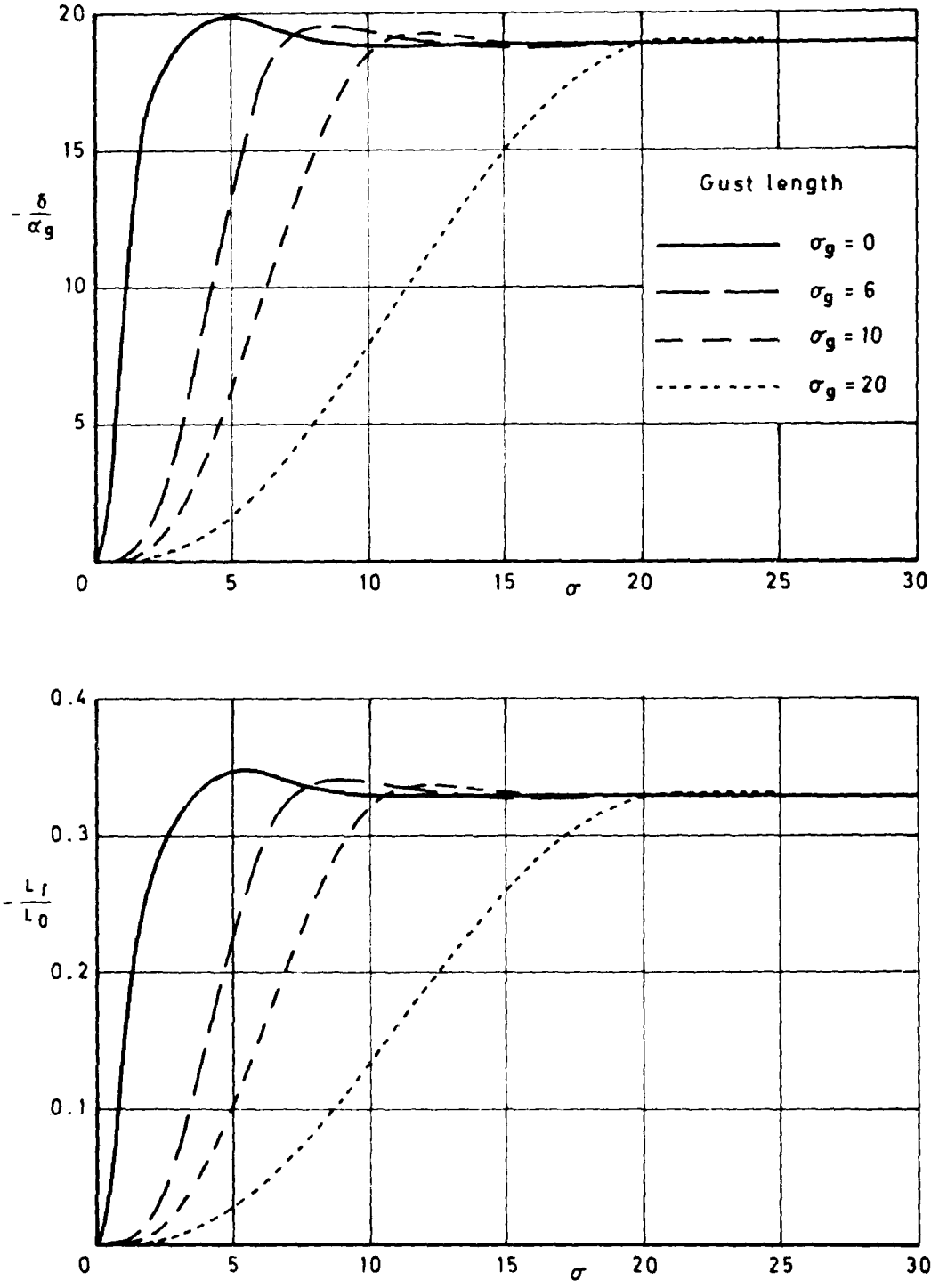

Fig 19 Control angles and tailplane lift at $x_T = 3\bar{c}$ to neutralize wing forces through various symmetric (1–cosine) gusts

TR 81157

Fig 20

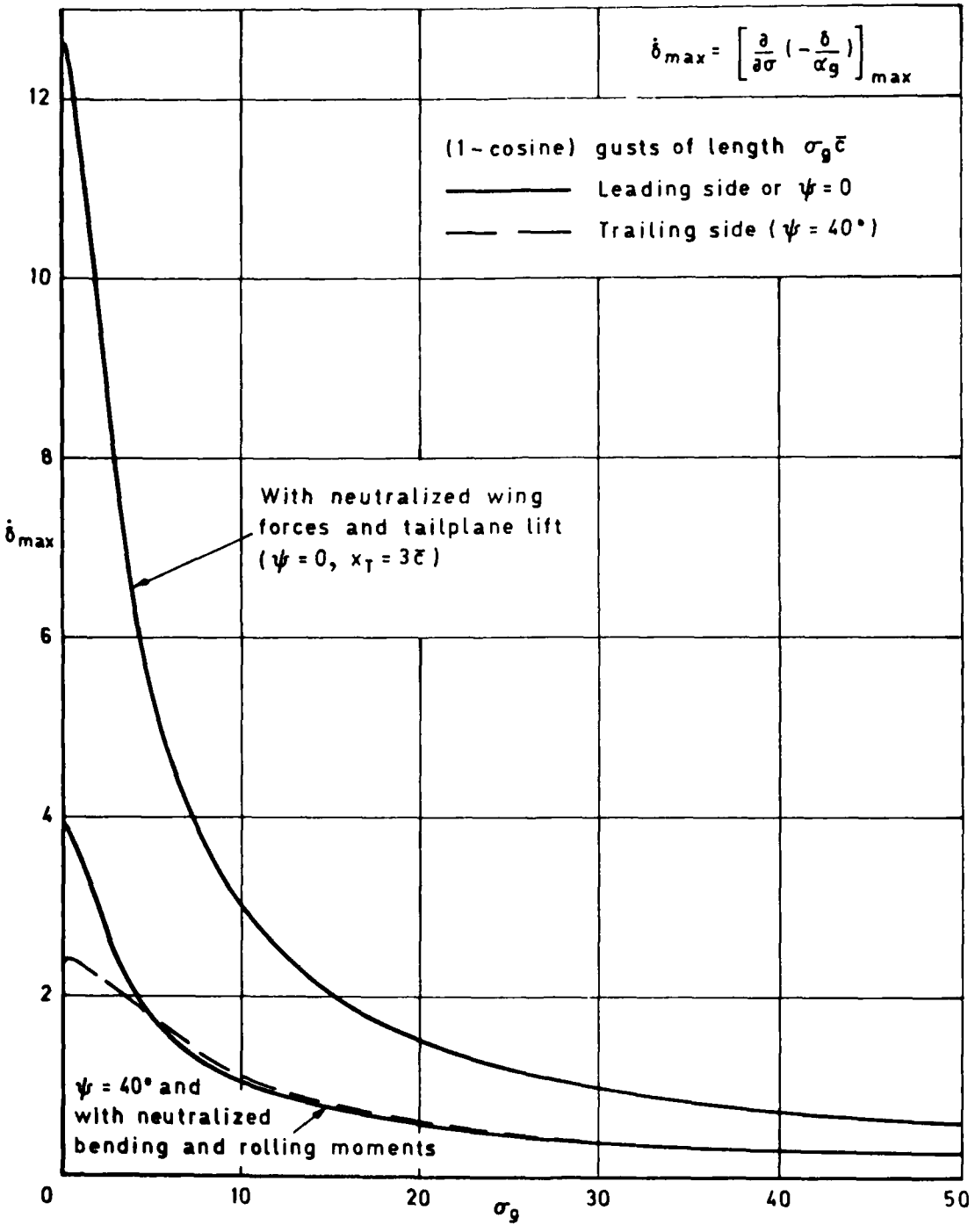

Fig 20 Influence of gust length on maximum control rates

TH 81157

REPORT DOCUMENTATION PAGE

Overall security classification of this page

UNCLASSIFIED

As far as possible this page should contain only unclassified information. If it is necessary to enter classified information, the box above must be marked to indicate the classification, e.g. Restricted, Confidential or Secret.

1. DRIC Reference (to be added by DRIC)	2. Originator's Reference	3. Agency Reference	4. Report Security Classification/Marking
	RAE TR 81157	N/A	UNCLASSIFIED

5. DRIC Code for Originator	6. Originator (Corporate Author) Name and Location
7673000W	Royal Aircraft Establishment, Farnborough, Hants, UK
5a. Sponsoring Agency's Code	6a. Sponsoring Agency (Contract Authority) Name and Location
N/A	N/A

7. Title Numerical aerodynamic studies of asymmetric gust entry

7a. (For Translations) Title in Foreign Language

7b. (For Conference Papers) Title, Place and Date of Conference

8. Author 1. Surname, Initials	9a. Author 2	9b. Authors 3, 4	10. Date	Pages	Refs.
Garner, H.C.	-	-	January 1982	52	9

11. Contract Number	12. Period	13. Project	14. Other Reference Nos.
N/A	N/A		Structures BF/B/920

15. Distribution statement
(a) Controlled by –
(b) Special limitations (if any) –

16. Descriptors (Keywords) (Descriptors marked * are selected from TEST)

Active controls. Aerodynamic loads*. Discrete gusts. Potential theory*. Subsonic flow*. Three-dimensional flow*. Unsteady flow*.

17. Abstract

Lifting-surface calculations for a particular wing at Mach number 0.8 are used to examine the aerodynamic consequences when one side of an aircraft enters a vertical gust before the other. The growth of lift, pitching moment, aileron hinge moment and the behaviour of the transient rolling moment are analysed. Their dependence on the inclination of the gust front and the length of a (1-cosine) gust is discussed.

Some idealized calculations of control-surface motion to suppress the wing root bending moment or to achieve undisturbed flight show only minor effects of gust inclination on control demand. But the transient rolling moment from asymmetric entry into a (1-cosine) gust within the spectrum of current airworthiness requirements is large enough to constitute a considerable handling problem. Ride control studies to eliminate heave, pitch and roll by means of two ailerons and an auxiliary tailplane or canard reveal distinct advantages of the canard as an active control.

END

DATE
FILMED

7-82

DTIC